



Original article

Mixed-ligand Cu(II)–vanillin Schiff base complexes; effect of coligands on their DNA binding, DNA cleavage, SOD mimetic and anticancer activity

Sartaj Tabassum^{a,*}, Samira Amir^a, Farukh Arjmand^a, Claudio Pettinari^{b,**}, Fabio Marchetti^c, Norberto Masciocchi^d, Giulio Lupidi^b, Riccardo Pettinari^b^a Department of Chemistry, Aligarh Muslim University (AMU), UP 202002, India^b School of Pharmacy, Via S. Agostino 1, University of Camerino, I-62032 Camerino (MC), Italy^c School of Science and Technology, Via S. Agostino 1, University of Camerino, I-62032 Camerino (MC), Italy^d Department of Chemical and Environmental Sciences, University of Insubria, Via Valleggio 11, 22100 Como, Italy

ARTICLE INFO

Article history:

Received 20 November 2011

Received in revised form

26 July 2012

Accepted 13 August 2012

Available online 23 August 2012

Keywords:

Coligands

DNA binding

SOD activity

Antitumor activity

ABSTRACT

SOD mimics with varying coligand are momentous in developing potential chemotherapeutic drugs. Cu(II) based SOD mimics **1–4** [CuLH(OAc)(H₂O)Y] (LH = 2-((E)-(1,3-dihydroxy-2-methylpropan-2-ylimino)methyl)-6-methoxyphenol, OAc = CH₃COO, **1**: Y = H₂O; **2**: Y = phen (1,10-phenanthroline), **3**: Y = tpimH (2,4,5-triphenylimidazole); **4**: Y = tfbimH (2-(trifluoromethyl)benzimidazole) were synthesized and thoroughly characterized. Their interaction with CT-DNA showed different non-covalent binding behaviour. SOD activity of **2** was highest among **1–4** which was further validated by gel electrophoresis. The pBR322 plasmid strand break offered by **2** + O₂^{•-} system reveals oxidative cleavage mechanism. *In vitro* antimicrobial activity of **1–4** was shown by percent inhibition data while *in vitro* anticancer activity of **1–4** was screened using 16 human carcinoma cell lines of different histological origin. Complex **2** showed higher efficacy towards 14 cell lines.

© 2012 Published by Elsevier Masson SAS.

1. Introduction

In recent years there has been a rapid expansion in the development of metal complexes as extensive diagnostic agents/chemotherapeutic drugs [1]. In this regard therapeutic agents that pertain to less toxic and more effective metallic component like Cu(II) are of particular interest and include a plethora of compounds: antitumor, antioxidant, antimicrobial and anti-inflammatory agents [2]. The appropriate redox property of Cu(II) is essential for various metabolic pathways like mitochondrial respiration, free radical scavenging, and iron absorption where it acts as a catalytic cofactor [3]. The Cu(II) complexes follows different mode of action towards DNA (non-covalent) as compared to cisplatin (covalent). Therefore, Cu(II)-based generic complexes exhibit higher antineoplastic potency towards human ovarian carcinoma (CH1), murine leukaemia (L1210), and various cervico-uterine carcinomas as compared to cisplatin [4,5]. A large number of chemotherapeutic agents and cytokines imply potentially useful

therapeutic strategies and elicit antitumor effect by inducing cancer cell apoptosis by generating large amount of noxious radicals into the cancer cells [6,7]. SOD can putatively participate in such apoptotic events leading to tumor reduction and cell proliferation.

Cu(II)containing SOD enzyme, Cu₂, Zn₂SOD is the most efficient catalytic species found in the mammalian cell plasma and extracellular spaces. It catalyzes the dismutation of superoxide radical (O₂^{•-}) and converts it into molecular oxygen and hydrogen peroxide via one electron redox cycle involving its Cu(II) centre. Since cancer cells have been investigated for rates of metabolism and generate large amount of intracellular O₂^{•-} as compared to normal cells [8], the SOD activity in cancer cell is lower than the normal cell [9]. SOD mimic enzyme affects tumor cell proliferation, due to the generation of increased amount of H₂O₂ and its metabolite OH[•] radical (formed via Fenton's reaction), which crucially causes cytotoxicity in affected cell lines [10]. Thus synthetic SOD mimics can be considered as a perfect tool in mediating apoptosis by implying oxidative stress induced by OH[•] radical.

Lippard et al. [11] have described a number of imidazolate-bridged homo and heterodinuclear SOD mimics and much of the attention has been laid towards their structure activity relationship. Such model complexes are often constructed by self-assembly of one or two complex units by the incorporation of imidazole bridge

* Corresponding author. Tel.: +91 9358255791.

** Corresponding author. Tel.: +39 0737 402234; fax: +39 0737 637345.

E-mail addresses: tsartaj62@yahoo.com (S. Tabassum), claudio.pettinari@unicam.it (C. Pettinari).

between both the units. However, the labile nature of bimetallic Cu(II) and Zn(II) complexes led the dissociation of self-assembled structures and made it difficult to study in detail their solution studies and SOD functions [12]. This is a prerequisite for the synthesis of monometallic SOD mimic complexes. The crystal structure of native Cu, Zn–SOD reported by J. A. Tainer et al. have also revealed Cu(II) as the active site of the enzyme [13]. The penta coordinated geometry around Cu(II) centre with a water molecule attached to the Arg 141 residue through hydrogen bonding is believed to facilitate the transportation of superoxide anion to the active site of the enzyme. The present work embodies the design and application of mononuclear penta coordinated Cu(II) complexes that have low molecular weight and provides models for metalloprotein (SOD) active sites by facilitating hydrogen bonding in the outer coordination sphere of the redox active centre for O_2^- stabilization [14–16].

The presence of different substituents in the intercalative ligand could affect changes in space configuration and in the electron density distribution around transition metal complexes, which not only influence their spectral properties but renders a clear understanding in evaluating the changes in SOD-like activity, as well as in the binding mechanism of transition metal complexes to DNA. The presence of coordination sites belonging to nitrogen heteroatomic rings such as imidazole, pyrazole, 1,10-phenanthroline, 2,2'-bipyridine, pyridine etc are considered important for high SOD activity and possess remarkable DNA binding propensity [17,18]. Among these coligands, phen (1,10-phenanthroline), is an important moiety which has attracted considerable attention for its versatility in exhibiting electronic properties and high cleavage efficiency [19]; tpimH, (2,4,5-triphenylimidazole), the imidazole derivative is an important domain present in histidyl residues of metalloprotein and possess several metal binding sites and tfbimH, (2-trifluoromethylbenzimidazole), a member of the benzimidazole family which can yield complexes that could serve as model compounds for purine nucleobases [20] and selectively inhibit endothelial cell growth and suppress angiogenesis *in vitro* and *in vivo* [21].

To ascertain the therapeutic potential of Cu(II)-based SOD mimics, we have carried out a systematic study on the Cu(II) Schiff

base complexes derived from *o*-vanillin and pro-ligand: 2-amino-2-methylpropane 1,3-diol with varying coligands. As illustrated in Chart 1, complexes exhibit novelty in structure due to presence of several pharmacophore-active sites that mimics native SOD enzyme viz., i) two free hydroxyl group of the ligand has been introduced as hydrogen bonding site pertained to guanidinium group in the Arg residue of native bovine Cu, Zn–SOD; ii) nitrogen containing heterocyclic units have been considered as a structural model of His residues; iii) distorted structure around Cu(II) provides feasible condition for the attack of O_2^- [22]. Beside determining the SOD activity of these Cu(II) ternary systems with varying coligands, other parameters viz., DNA binding, nuclease, antimicrobial and anti-tumor activities were also evaluated thoroughly.

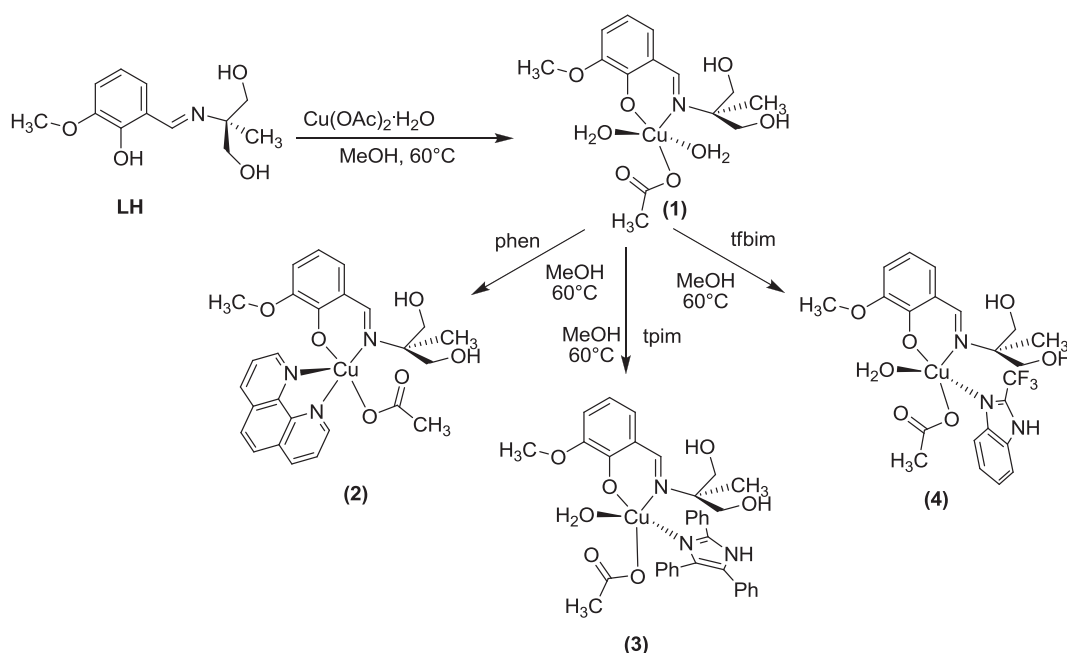
2. Chemistry

The Cu(II) complex $[Cu(LH)(OAc)(H_2O)_2]$ was synthesized by mixing stoichiometric amounts of $Cu(OAc)_2 \cdot H_2O$ with Schiff base LH in methanol (Scheme 1). The final Rietveld refinement plot of the ligand LH, is shown in Fig. 1. The preformed complex $[Cu(LH)(OAc)(H_2O)_2]$ was further reacted with coligands: phen, tpimH and tfbimH to yield the ternary complexes $[Cu(LH)(phen)(OAc)]$, $[Cu(LH)(tpimH)(OAc)(H_2O)]$ and $[Cu(LH)(tfbimH)(OAc)(H_2O)]$, respectively by removal of water molecule from the coordination sphere of Cu(II) ion. The proposed structures of complexes (Fig. 2) were established by elemental analysis and spectroscopic studies (UV–visible, IR, conductivity, mass spectra, EPR and magnetic susceptibility measurements). All the complexes are soluble in common organic solvents. The molar conductivity (Λ_M) data of all complexes is consistent with their non-electrolytic nature.

3. Pharmacology

3.1. Proposed mechanistic pathway of reactive oxygen species responsible for DNA cleavage

DNA cleavage mediated by complex $[Cu(LH)(Y)(OAc)]$ is similar to that proposed for other multinuclear Cu(II) complexes [23,24].



Scheme 1. Proposed scheme for the synthesis of complexes 1–4.

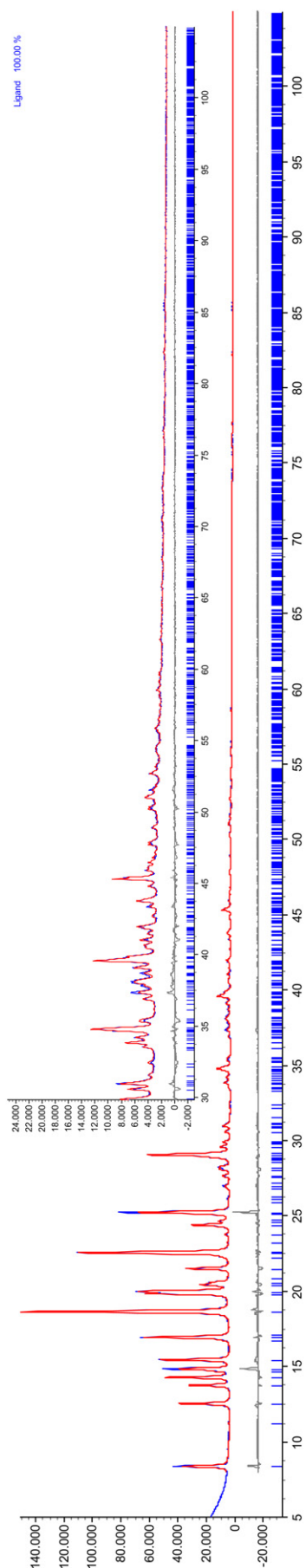
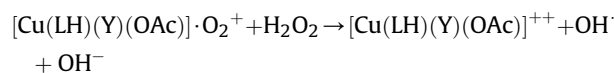
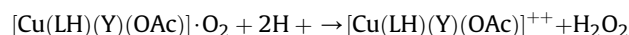
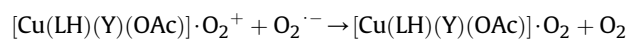
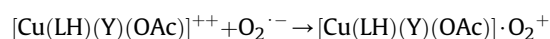


Fig. 1. Final Rietveld refinement plot for species LH, with difference plot and peak markers at the bottom. The insert shows the high angle region at a magnified scale (5×).

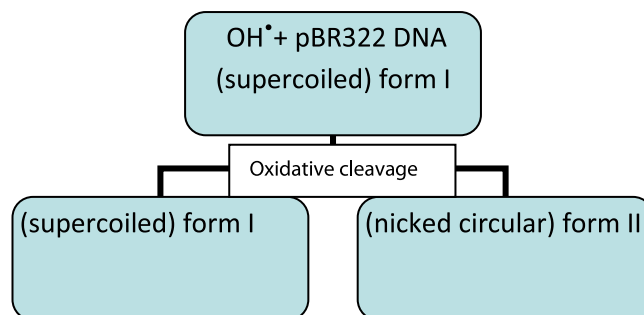
Complexes **1–4**, fulfils every criterion to behave as potent SOD mimic by various reasons. Firstly, Cu(II) center are initially reduced to Cu(I) which further reacts with dioxygen to form a peroxodicopper(II) derivative, and could generate active oxygen species required for cleavage. The reaction proceeds through preliminary steps. Step 1: formation of dioxygen by superoxide causing redox changes at the metal centre either by i) superoxide coordination to the metal ion (inner sphere) prior to electron transfer or ii) direct electron transfer to the outer sphere of metal ion without coordination as shown in Fig. 3 [25]. Step 2: formation of H_2O_2 by the oxidation of $\text{O}_2^{\cdot-}$ in presence of redox active metal centre leads to proton-coupled electron transfer. For this purpose, metal ion should possess “vacant” coordination site that can directly bind to $\text{O}_2^{\cdot-}$ in its coordination sphere. In complexes **1–4**, the free ‘vacant site’ is facilitated by square pyramidal geometry of these complexes favouring direct $\text{O}_2^{\cdot-}$ binding.

Another aspect for a complex to show SOD activity depends upon the availability of labile ligand in complex structure. It has been cited in the literature that the axial site of Cu(II) complex that consists of solvent molecules with little steric hindrance, undergoes a fast attachment of $\text{O}_2^{\cdot-}$ at the Cu(II) centre [26]. Complexes **1**, **3**, and **4** possesses labile water molecules coordinated to the Cu(II) centre and could provides excellent locus for $\text{O}_2^{\cdot-}$ attachment. Third possibility of $\text{O}_2^{\cdot-}$ binding to the complex is based upon the investigation of A. Klanicova et al. [27]. Their proposed mechanism involves the substitution of the ligand (other than N donor ligands i.e. coordinated perchlorate) by $\text{O}_2^{\cdot-}$ with the formation of a superoxo-complex. Moreover, the reduction of Cu(II) to Cu(I) occurs, with the concomitant release of O_2 forming tetracoordinated Cu(I) species. This, Cu(I) species interact with another $\text{O}_2^{\cdot-}$ and re-oxidizes to Cu(II) species forming H_2O_2 molecule. Again, this particular condition could be applied to the complexes **1–4** and is likely that the coordinated acetate ligand in these complexes could be easily substituted by $\text{O}_2^{\cdot-}$. Thus, to a greater extent, our complexes represent the (mechanism) active center of native Cu, Zn–SOD.

The general $\text{O}_2^{\cdot-}$ attack could be described as:



The OH^{\cdot} formation leads to the oxidative cleavage of pBR322 DNA.



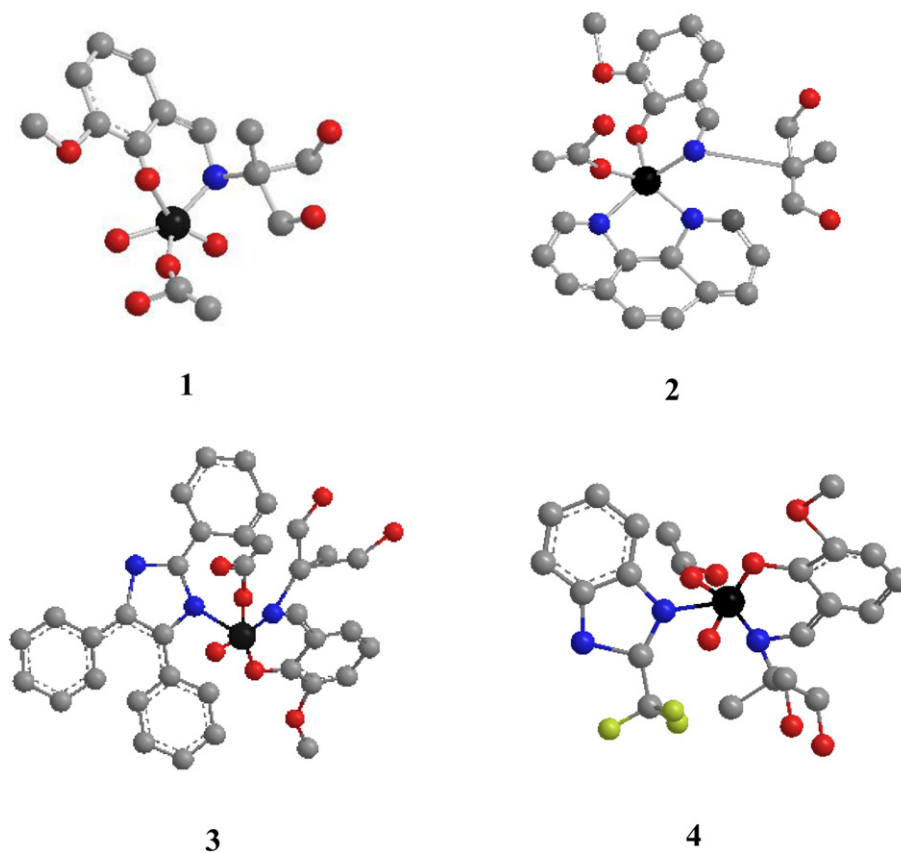


Fig. 2. Cylindrical bonded three dimensional model of metal complex $[\text{Cu}(\text{LH})(\text{OAc})(\text{H}_2\text{O})_2](1)$, $[\text{Cu}(\text{LH})(\text{Phen})(\text{OAc})](2)$, $[\text{Cu}(\text{LH})(\text{tpimH})(\text{OAc})(\text{H}_2\text{O})](3)$ and $[\text{Cu}(\text{LH})(\text{tfbimH})(\text{OAc})(\text{H}_2\text{O})](4)$. Colour scheme: N dark blue; O red; C grey; F light green and Cu(II) dark grey; H atoms are omitted for clarity. (For interpretation of the references to colour in this figure legend, the reader is referred to the web version of this article.)

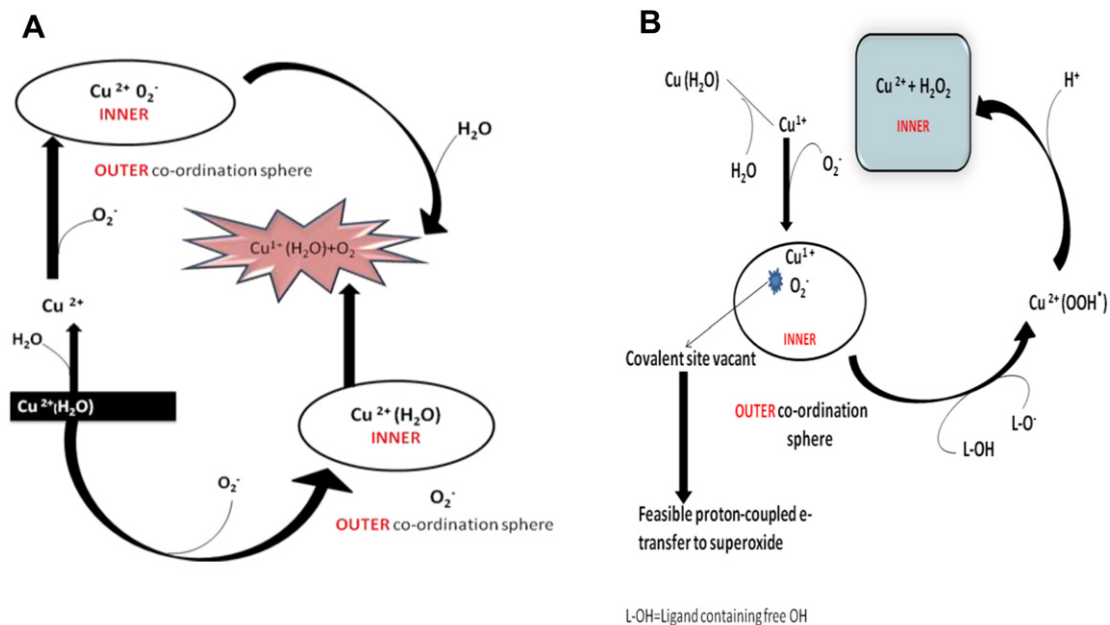


Fig. 3. Diagrammatic representation of dioxygen formation by superoxide anion via inner and outer coordination sphere (A), and oxidation by superoxide to give hydrogen peroxide (B).

4. Results and discussion

4.1. IR spectroscopy

The IR spectrum of the ligand LH exhibited characteristic azomethine band $\nu(\text{HC}=\text{N}-)$ at 1637 cm^{-1} while intermolecular H-bonded phenolic $-\text{OH}$ and $\nu(\text{C}-\text{O})$ were observed at 2602 cm^{-1} and 1466 cm^{-1} , respectively [28]. The IR spectra of complexes $[\text{Cu}(\text{LH})(\text{OAc})(\text{H}_2\text{O})_2]$, $[\text{Cu}(\text{LH})(\text{phen})(\text{OAc})]$, $[\text{Cu}(\text{LH})(\text{tpimH})(\text{OAc})(\text{H}_2\text{O})]$ and $[\text{Cu}(\text{LH})(\text{tfbimH})(\text{OAc})(\text{H}_2\text{O})]$ undergoes a relative decrease in $\nu(\text{HC}=\text{N}-)$ frequency in the range $1621\text{--}1626\text{ cm}^{-1}$ supportive of the coordination of imine nitrogen to Cu(II) ion [29]. The shift of phenolic $\nu(\text{C}-\text{O})$ from 1466 cm^{-1} to lower wavenumber $1438\text{--}1440\text{ cm}^{-1}$ in the studied complexes has been attributed to the coordination of phenolic oxygen to the Cu(II) ion [30]. The extent of the separation between carboxylate stretches ($\Delta = \nu_{\text{as}}(\text{COO}^-) - \nu_{\text{s}}(\text{COO}^-)$) of the acetate, determines binding mode of carboxylate [31]. The following criteria can be used for Δ values of carboxylate complexes of divalent metal cations.

$\Delta(\text{monodentate}) > \Delta(\text{ionic}) > \Delta(\text{bridging bidentate}) > \Delta(\text{chelating bidentate})$.

Usually Δ value of $\sim 170\text{ cm}^{-1}$ corresponds to ionic carboxylate group, while the $\Delta \sim 187\text{--}200\text{ cm}^{-1}$ indicates monodentate coordination [32]. Upon complexation, change in the force field around the metal atom causes redistribution of the electron density which shifts $\nu_{\text{as}}(\text{COO}^-)$ to higher wave number with respect to ionic acetates ($\Delta \sim 170\text{ cm}^{-1}$) and leads to monodentate coordination of acetates. However, the shifting of $\nu_{\text{as}}(\text{COO}^-)$ to lower wavenumbers with respect to the ionic group leads to bidentate acetates ($\Delta < 170\text{ cm}^{-1}$). The $\nu_{\text{as}}(\text{COO}^-)$ for 'bridging' and ionic acetates shows slight difference in their frequencies [33].

The Δ values of all the studied complexes lie in the range $201\text{--}287\text{ cm}^{-1}$ suggestive of monodentate coordination of the acetate to the Cu(II) ion. The presence of coordinated water molecules in complexes $[\text{Cu}(\text{LH})(\text{OAc})(\text{H}_2\text{O})_2]$, $[\text{Cu}(\text{LH})(\text{tpimH})(\text{OAc})(\text{H}_2\text{O})]$ and $[\text{Cu}(\text{LH})(\text{tfbimH})(\text{OAc})(\text{H}_2\text{O})]$ were ascertained by rocking mode in the region $840\text{--}860\text{ cm}^{-1}$ [34]. In complex $[\text{Cu}(\text{LH})(\text{phen})(\text{OAc})]$, the aromatic (Phen) stretching vibrations $\nu(\text{C}=\text{C})$ and $\nu(\text{C}=\text{N})$ were observed at 1429 and 1516 cm^{-1} , respectively. The complex $[\text{Cu}(\text{LH})(\text{tpimH})(\text{OAc})(\text{H}_2\text{O})]$ displays a strong band at 695 cm^{-1} due to out of plane mode of tpimH ring. Moreover, the $\nu(\text{C}=\text{N})$ vibrations of the imidazole ring in complexes $[\text{Cu}(\text{LH})(\text{tpimH})(\text{OAc})(\text{H}_2\text{O})]$ and $[\text{Cu}(\text{LH})(\text{tfbimH})(\text{OAc})(\text{H}_2\text{O})]$ lie in the range $1400\text{--}1500\text{ cm}^{-1}$ [35]. A strong band at 1128 cm^{-1} observed in the complex $[\text{Cu}(\text{LH})(\text{tfbimH})(\text{OAc})(\text{H}_2\text{O})]$ corresponds to C–F vibration [36]. The far IR spectra of the complexes exhibited absorption bands, $500\text{--}600\text{ cm}^{-1}$, $410\text{--}480\text{ cm}^{-1}$ assigned to Cu–O and Cu–N stretching vibrations [37].

4.2. Magnetic susceptibility studies

The magnetic susceptibility values for complexes $[\text{Cu}(\text{LH})(\text{OAc})(\text{H}_2\text{O})_2]$, $[\text{Cu}(\text{LH})(\text{phen})(\text{OAc})]$, $[\text{Cu}(\text{LH})(\text{tpimH})(\text{OAc})(\text{H}_2\text{O})]$ and $[\text{Cu}(\text{LH})(\text{tfbimH})(\text{OAc})(\text{H}_2\text{O})]$, at room temperature lies in the range of $1.8\text{--}1.9\text{ BM}$ which correspond to one unpaired electron and are consistent with the d^9 configuration around Cu(II) ion [38].

4.3. EPR spectra

In the absence of single crystal EPR analysis, reliable parameters for Cu(II) complex can be obtained by running the solution EPR spectrum as a frozen glass. Since powdered samples are sufficiently

crystalline, the orientation of their spins in the material are not truly random. Thus, powder samples can sometimes give misleading g values due to the presence of significant bipolar interactions between molecules in the sample. The X-band EPR spectra of the Cu(II) complexes $[\text{Cu}(\text{LH})(\text{OAc})(\text{H}_2\text{O})_2]$, $[\text{Cu}(\text{LH})(\text{phen})(\text{OAc})]$, $[\text{Cu}(\text{LH})(\text{tpimH})(\text{OAc})(\text{H}_2\text{O})]$ and $[\text{Cu}(\text{LH})(\text{tfbimH})(\text{OAc})(\text{H}_2\text{O})]$, were recorded at 133 K with a magnetic field strength of $3000 \pm 1000\text{ G}$. All the complexes showed anisotropic spectra with $g_{\parallel} = 2.26$, $g_{\perp} = 2.02$ and $A_{\parallel} = 176$ for complex $[\text{Cu}(\text{LH})(\text{OAc})(\text{H}_2\text{O})_2]$. Complex $[\text{Cu}(\text{LH})(\text{phen})(\text{OAc})]$ exhibits $g_{\parallel} = 2.25$, $g_{\perp} = 2.01$ and $A_{\parallel} = 183$ (Fig. 4). For complex $[\text{Cu}(\text{LH})(\text{tpimH})(\text{OAc})(\text{H}_2\text{O})]$ the EPR spectrum reveals $g_{\parallel} = 2.22$, $g_{\perp} = 2.01$ and $A_{\parallel} = 183$ while complex $[\text{Cu}(\text{LH})(\text{tfbimH})(\text{OAc})(\text{H}_2\text{O})]$ have $g_{\parallel} = 2.22$, $g_{\perp} = 2.01$ and $A_{\parallel} = 183$, respectively. In solution, individual molecule persist true random orientations that are well separated from one another. Therefore, EPR spectra remains unaffected. Since $g_{\parallel} > g_{\perp} > 2.0023$ reveals that the unpaired electron is present in the $dx^2 - y^2$ orbital and is consistent with Cu(II) ion in a square pyramidal geometry [39a]. The values of g_{\parallel} lie in the range $2.22\text{--}2.28$, suggesting the presence of a CuN_2O_2 chromophore [40] in solution and also $g_{\parallel} < 2.3$ indicates an appreciable metal-ligand covalent character [41,42].

4.4. Electronic absorption spectra

The UV–vis spectra of complexes **1–4** was measured at room temperature in the region $190\text{--}1100\text{ nm}$ showing distinct regions. The electronic intra-ligand $\pi\text{--}\pi^*$ and LMCT transitions were observed in the region $202\text{--}278\text{ nm}$ and $368\text{--}381\text{ nm}$, respectively. However, d–d transitions observed in the region $633\text{--}675\text{ nm}$ are typical for penta coordinated Cu(II) complexes having a distorted square pyramidal geometry ($d_{xz}, d_{yz} \rightarrow d_{x^2-y^2}$) [43].

4.5. Crystal structure of LH

The ligand LH crystallizes in the triclinic space group with one crystallographically independent molecule, shown in Fig. 5. As described in the experimental section, within the molecule, only torsional angles were free, which resulted in the following conformational parameters: $\text{C}5\text{--}\text{C}6\text{--}\text{C}8=\text{N}1$ $176.7(4)^\circ$ (maintaining the iminic group nearly coplanar with the π -system of the phenyl residue) $\text{C}6\text{--}\text{C}8=\text{N}1\text{--}\text{C}9$ $176.4(2)^\circ$ (in agreement with the trans-configuration of the iminic moiety) and $\text{C}1\text{--}\text{O}1\text{--}\text{C}2\text{--}\text{C}7$ $175.3(4)^\circ$, indicating the anti-disposition of the OMe group with respect to the other (adjacent) substituents. Interestingly, the ligand LH shows a strong intramolecular H-bond between O2 and N1 ($\text{O}1\cdots\text{N}1$ 2.50 \AA), along with several intramolecular bonds

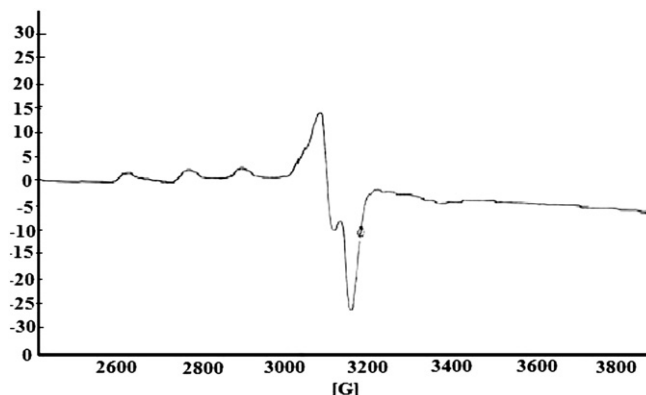


Fig. 4. EPR spectra of complex $[\text{Cu}(\text{L})(\text{phen})(\text{OAc})(\text{H}_2\text{O})](2)$ in methanol at 133 K .

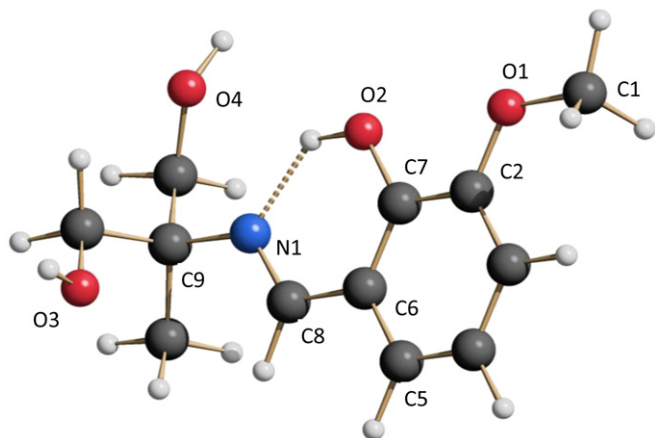


Fig. 5. Schematic drawing of the molecule of LH (with partial labelling scheme), showing the conformation derived from our X-ray powder diffraction study. Colour code: carbon (grey); nitrogen (blue); oxygen (red); hydrogen (white). The fragmented line indicates the intramolecular H-bond interaction. (For interpretation of the references to colour in this figure legend, the reader is referred to the web version of this article.)

(O2...O3 and O2...O4 of 2.71 and 2.70 Å, respectively) granting an efficient packing and a high melting point (165 °C).

Accordingly, O2 is tetraconnected (with three H-bond interactions in nearly tetrahedral geometry), while the O3 and O4 atoms, belonging to a more peripheral section of the molecule, and show a single H-bond interaction. Inter alia, this conformational analysis, as well as the determination of the main crystal packing features, witness the high quality of our powder diffraction study, which, although coping with idealized bond distances and angles (derived from simple molecular mechanics optimization), was nevertheless able to rescue important, otherwise inaccessible, structural features (no single-crystal of suitable quality being available).

5. DNA-binding mode and affinity

5.1. Absorption spectral studies

Electronic absorption spectroscopy is employed to examine the binding mode of CT-DNA with small molecules [44]. The absorption spectra of complexes [Cu(LH)(OAc)(H₂O)₂], [Cu(LH)(phen)(OAc)], [Cu(LH)(tpimH)(OAc)(H₂O)] and [Cu(LH)(tfbimH)(OAc)(H₂O)] with CT-DNA were depicted in Fig. 6. A fixed concentration of the complexes were titrated with increasing concentration of CT-DNA ($R = [\text{DNA}]/[\text{Cu}] = 1\text{--}40$). It was observed that the complex [Cu(LH)(OAc)(H₂O)₂] exhibited 'hyperchromism' in the intra-ligand region (at 278 nm) with a noticeable blue shift of 10 nm (Table 1). This indicates strong binding propensity of the complex towards CT-DNA (non-covalent interactions) leading to the damaged DNA double helix structure. Complex [Cu(LH)(phen)(OAc)] also displayed 'hyperchromism' with the blue shift of 8 nm in the same region (at 273 nm) (Fig. 6B). In general, 'hyperchromism' and blue shift suggests the corresponding (conformational and structural) changes after the complexes are bound to CT-DNA electrostatically via external contact (surface binding) with the DNA duplex. While 'hypochromism' and a red shift (bathochromism) of absorption band implicates intercalative mode of binding and is likely that the metal complexes with aromatic chromophore stabilizes the DNA duplex [45,46]. However, 'hyperchromism' obtained for complex [Cu(LH)(phen)(OAc)] is characteristic of the complex bound to DNA through non-covalent interactions or the complex could uncoil the helix and made more bases embedded in the DNA explored [47].

On contrary, complexes [Cu(LH)(tpimH)(OAc)(H₂O)] and [Cu(LH)(tfbimH)(OAc)(H₂O)] exhibited both 'hyperchromic' and 'hypochromic effect' at intra-ligand and LMCT regions. Upon addition of increasing concentration of CT-DNA to the complex [Cu(LH)(tpimH)(OAc)(H₂O)] and [Cu(LH)(tfbimH)(OAc)(H₂O)], 'hyperchromism' was observed in the intra-ligand region (277–278 nm) with a blue shift of 12 nm and 10 nm, respectively. Appreciable changes in the position of the LMCT band in the region 371–372 nm were observed with the decreasing order of the band intensities, resulting into 'hypochromism' along with the red shift of 4–6 nm, respectively (Fig. 6C, D and C', D'). A distinct isosbestic point was observed at 310 nm for complex [Cu(LH)(tpimH)(OAc)(H₂O)] and 315 nm for complex [Cu(LH)(tfbimH)(OAc)(H₂O)] indicating intercalative mode of binding of these complexes to the double helix structure of DNA. The presence of aromatic chromophore viz., tpimH and tfbimH facilitates the stacking interaction of the complex with the base pair of DNA. The π^* orbital of the intercalated ligand couple with the π orbital of the DNA base, decreasing of the $\pi\text{--}\pi^*$ transitions energy which ultimately leads into the red shift [48]. To quantify the extent of DNA binding, the intrinsic binding constant K_b of the studied complexes with varying coligands were determined and the data were presented in Table 1 that shows either electrostatic and/or intercalative binding trends of the complexes 1, 3 and 4, respectively with CT-DNA. Complex 2, however possesses a planar aromatic moiety (phen) and the probability of binding of this complex to CT-DNA via partial intercalation cannot be ruled out ($K_b = 2.70 \times 10^4$), nonetheless 'hyperchromism' supports electrostatic interaction.

5.2. Steady state emission titrations

In absence of CT-DNA, all the complexes when excited between 265 and 268 nm, emitted luminescence in Tris–HCl buffer/pH 7.2, with emission bands observed in the range of 282–290 nm. Fixed amount of all the metal complexes were titrated with increasing amount of CT-DNA ($R = 40$), and as a consequence an increase in the emission intensity was observed for complexes 1–4 (Table 2). The hydrophobic molecular structure of CT-DNA could be responsible for enhancing the fluorescence quantum yield of complexes which in turn leads to the higher fluorescence intensity with increasing concentration of CT-DNA. The binding constant of the complexes were obtained from Stern–Volmer relationship [49] and followed the order, [Cu(LH)(phen)(OAc)] > [Cu(LH)(tfbimH)(OAc)(H₂O)] > [Cu(LH)(tpimH)(OAc)(H₂O)] > [Cu(LH)(OAc)(H₂O)₂]. The interaction of [Cu(LH)(phen)(OAc)] with CT-DNA displays a higher binding propensity ca. three times greater in magnitude as compared to other complexes (Fig. 7).

To evaluate the affinity of complexes towards CT-DNA, quenching experiments were performed using [Fe(CN)₆]⁴⁻ (Table 3) which reveal the binding strength of complexes with CT-DNA. The emission spectra with increasing concentration of the quencher are depicted in Fig. 8. The accessibility of DNA-bound exciplex to the quencher depends upon the strength of binding of complex to DNA. Stronger the binding, lesser the chances for availability of DNA-bound exciplex to the quencher and vice versa. The quenching efficiency is evaluated by using Stern–Volmer constant K_{sv} which follows the order [Cu(LH)(tfbimH)(OAc)(H₂O)] > [Cu(LH)(tpimH)(OAc)(H₂O)] > [Cu(LH)(phen)(OAc)] > [Cu(LH)(OAc)(H₂O)₂].

5.3. Viscosity measurements

Viscosity is considered as least ambiguous and most critical test in predicting the nature of binding of the complexes to CT-DNA, in absence of crystallographic data [50]. A classical intercalator causes

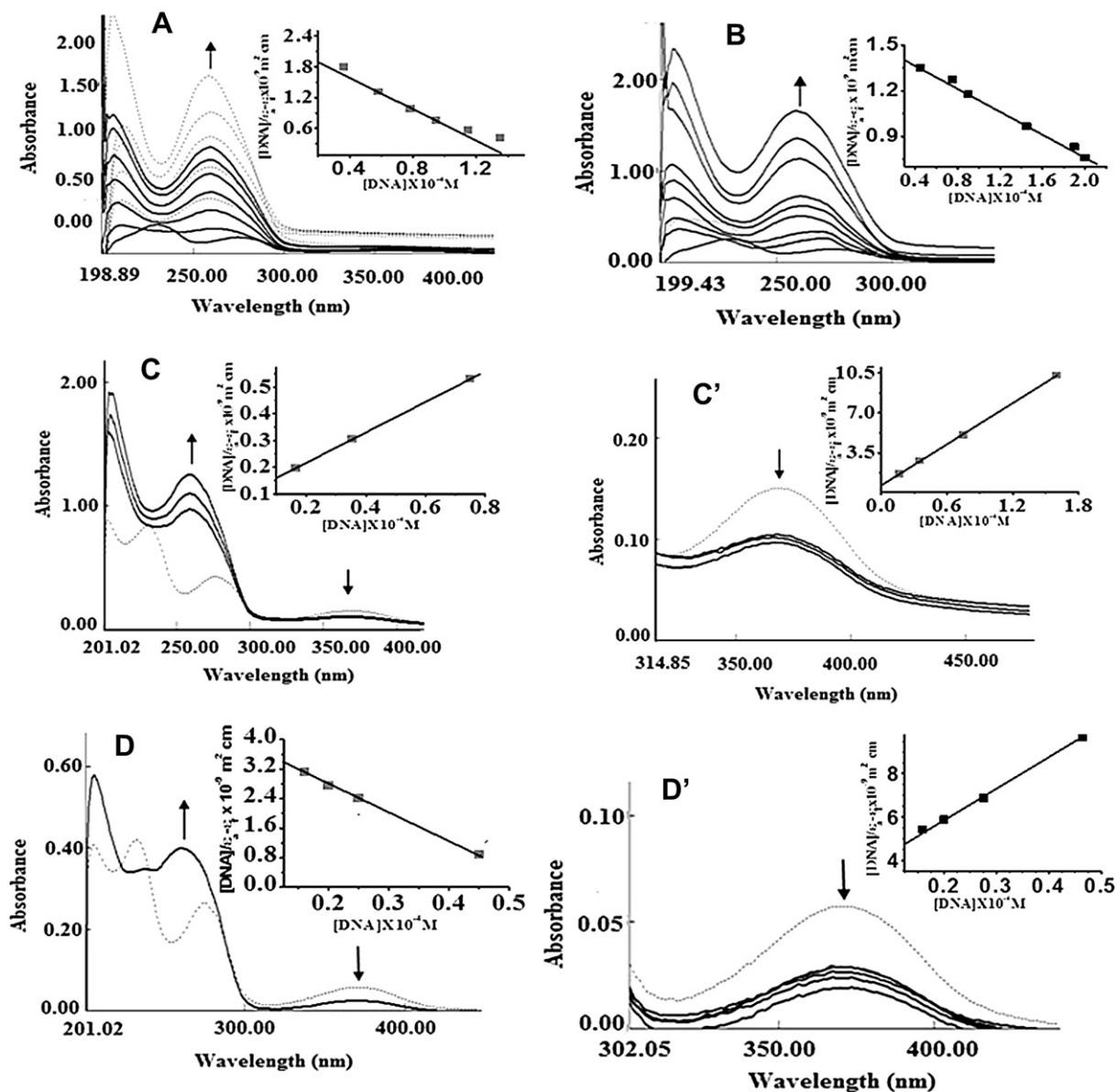


Fig. 6. Absorption spectral traces of complexes [Cu(L)(CH₃COO)(H₂O)₂](1), [Cu(L)(Phen)(CH₃COO)](2), [Cu(L)(tpimH)(CH₃COO)(H₂O)](3); C & C', [Cu(L)(tfbimH)(CH₃COO)(H₂O)](4); D & D' ([complex 1–4] = 1 × 10⁻⁵ M) in MeOH solution in the absence and presence of increasing amounts of CT-DNA ([CT-DNA] = 0–1.35 × 10⁻⁴ M). The arrows show the changes upon increasing amounts of CT-DNA. Inset: Plots of [DNA]/ε_f - ε_f (m² cm) vs [DNA] for the titration of CT-DNA with complexes 1–4; ■ experimental data points; full lines, linear fitting of the data. C' and D' represent the spectral changes of absorbance of complexes 3, and 4 in the range 315–475 nm ('Hypochromic effect').

significant increase in the viscosity of DNA solution due to the increase in the separation in overall DNA contour length [51]. A partial/or non-classical intercalation of metal complexes causes a bend or kink in the DNA helix reducing its effective length and, as

a result, DNA solution viscosity is decreased or remains unchanged [52,53]. In presence of increasing amount of complexes [Cu(L-H)(OAc)(H₂O)₂], [Cu(LH)(phen)(OAc)], [Cu(LH)(tpimH)(OAc)(H₂O)] and [Cu(LH)(tfbimH)(OAc)(H₂O)] the relative viscosity of CT-DNA

Table 1
Electronic spectral properties of Cu(II) complexes [Cu(LH)(OAc)(H₂O)₂](1), [Cu(LH)(phen)(OAc)](2), [Cu(LH)(tpimH)(OAc)(H₂O)](3) and [Cu(LH)(tfbimH)(OAc)(H₂O)](4) in presence of CT-DNA with mean standard deviation values.

Complex	Ligand based λ max (nm)		R ^a	Changes in absorbance (Δε%)	Shifts (nm)		K _b (M ⁻¹)
	π-π*	CT			Blue	Red	
1	278	—	27	Hyperchromism (84.46)	10	—	8.10 × 10 ³ (±0.04)
2	273	—	40	Hyperchromism (78.88)	8	—	2.70 × 10 ⁴ (±0.02)
3	278	—	32	Hyperchromism (56)	12	—	5.79 × 10 ⁴ (±0.04),
4	—	372	—	Hypochromism (66)	—	4	8.30 × 10 ⁴ (±0.02)
5	277	—	9	Hyperchromism (84)	10	—	6.10 × 10 ⁴ (±0.06),
5	—	371	—	Hypochromism (55)	—	6	4.06 × 10 ⁵ (±0.04)

^a R = [DNA]/[Cu complex] where concentration of Cu(II) solutions = 1 × 10⁻⁵ M.

Table 2

Emission properties of complexes [Cu(LH)(OAc)(H₂O)₂](**1**), [Cu(LH)(phen)(OAc)](**2**), [Cu(LH)(tpimH)(OAc)(H₂O)](**3**) and [Cu(LH)(tfbimH)(OAc)(H₂O)](**4**) bound to CT-DNA.

Complex	Excitation (nm)	Emission (nm)	<i>K</i> (M ⁻¹)
1	260	282	171 × 10 ⁴
2	260	284	6.39 × 10 ⁴
3	258	285	1.85 × 10 ⁴
4	265	290	2.95 × 10 ⁴

increases steadily (Fig. 9). In case of complex [Cu(LH)(OAc)(H₂O)₂] the increase in viscosity is less as compared to complexes [Cu(LH)(phen)(OAc)], [Cu(LH)(tpimH)(OAc)(H₂O)] and [Cu(LH)(tfbimH)(OAc)(H₂O)] in the same concentration ranges of CT-DNA. Thus, it is concluded that complexes [Cu(LH)(phen)(OAc)], [Cu(LH)(tpimH)(OAc)(H₂O)] and [Cu(LH)(tfbimH)(OAc)(H₂O)] exhibit higher affinity for the intercalative site on DNA as compared to complex [Cu(LH)(OAc)(H₂O)₂] that bring conformational changes due to partial intercalation of these complexes within the hydrophobic DNA pockets [54]. The increasing degree of viscosity follows the order [Cu(LH)(tfbimH)(OAc)(H₂O)] > [Cu(LH)(tpimH)(OAc)(H₂O)] > [Cu(LH)(phen)(OAc)] > [Cu(LH)(OAc)(H₂O)₂].

Table 3

Binding constant values for the quenching of [Fe(CN)₆]⁴⁻ with complexes [Cu(LH)(OAc)(H₂O)₂](**1**), [Cu(LH)(phen)(OAc)](**2**), [Cu(LH)(tpimH)(OAc)(H₂O)](**3**) and [Cu(LH)(tfbimH)(OAc)(H₂O)](**4**), in absence (A) and in the presence (B) of CT-DNA with mean standard deviation value.

Complex	<i>K</i> _{sv} (M ⁻¹) (A)	<i>K</i> _{sv} (M ⁻¹) (B)
1	3.28(±0.6) × 10 ⁴	2.4(±0.5) × 10 ⁴
2	4.21(±0.3) × 10 ⁴	2.21(±0.2) × 10 ⁴
3	5.14(±0.4) × 10 ⁴	2.78(±0.3) × 10 ⁴
4	8.17(±0.5) × 10 ⁴	2.82(±0.3) × 10 ⁴

5.4. Cyclic voltammetry

Electrochemical techniques are complementary to other related biophysical techniques that are applied to study the interaction between the redox active molecules and biomolecules [55]. Important criteria for a complex to act as SOD mimic is its metal-centred redox potential that facilitates catalytic disproportionation of O₂^{•-}. The cyclic voltammogram of complexes [Cu(LH)(OAc)(H₂O)₂], [Cu(LH)(phen)(OAc)], [Cu(LH)(tpimH)(OAc)(H₂O)] and [Cu(LH)(tfbimH)(OAc)(H₂O)] in absence and in the presence of CT-DNA were recorded in aqueous solutions with 0.4 M KNO₃ as

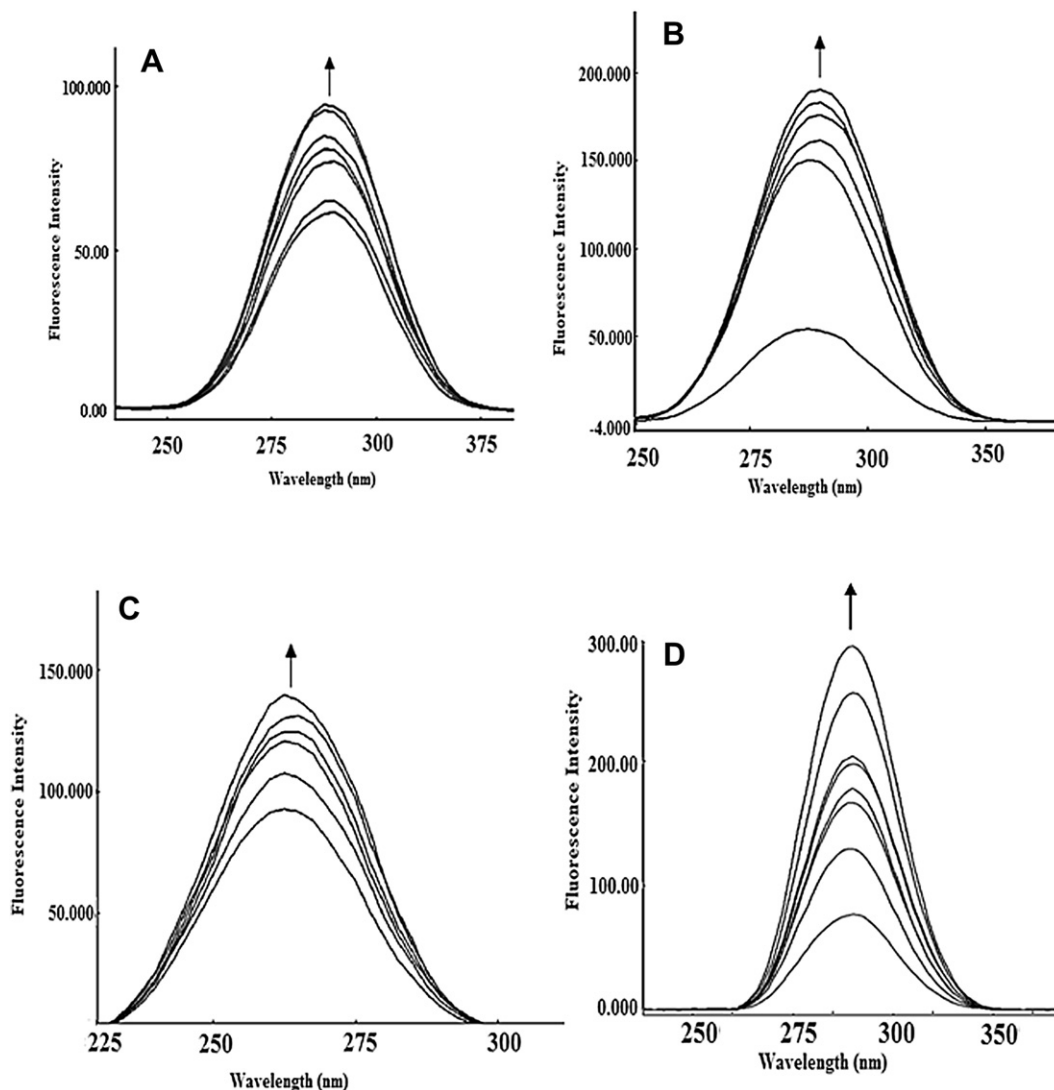


Fig. 7. Emission spectra of [Cu(L)(OAc)(H₂O)₂](**1**); A, [Cu(L)(Phen)(OAc)](**2**); B, [Cu(L)(tpimH)(OAc)(H₂O)](**3**); C and [Cu(L)(tfbimH)(OAc)(H₂O)](**4**); D in Tris–HCl buffer in the presence of CT-DNA. [CT-DNA] (0–1.35 × 10⁻⁴ M). Arrows show the intensity changes upon addition of the complexes (1 × 10⁻⁵ M).

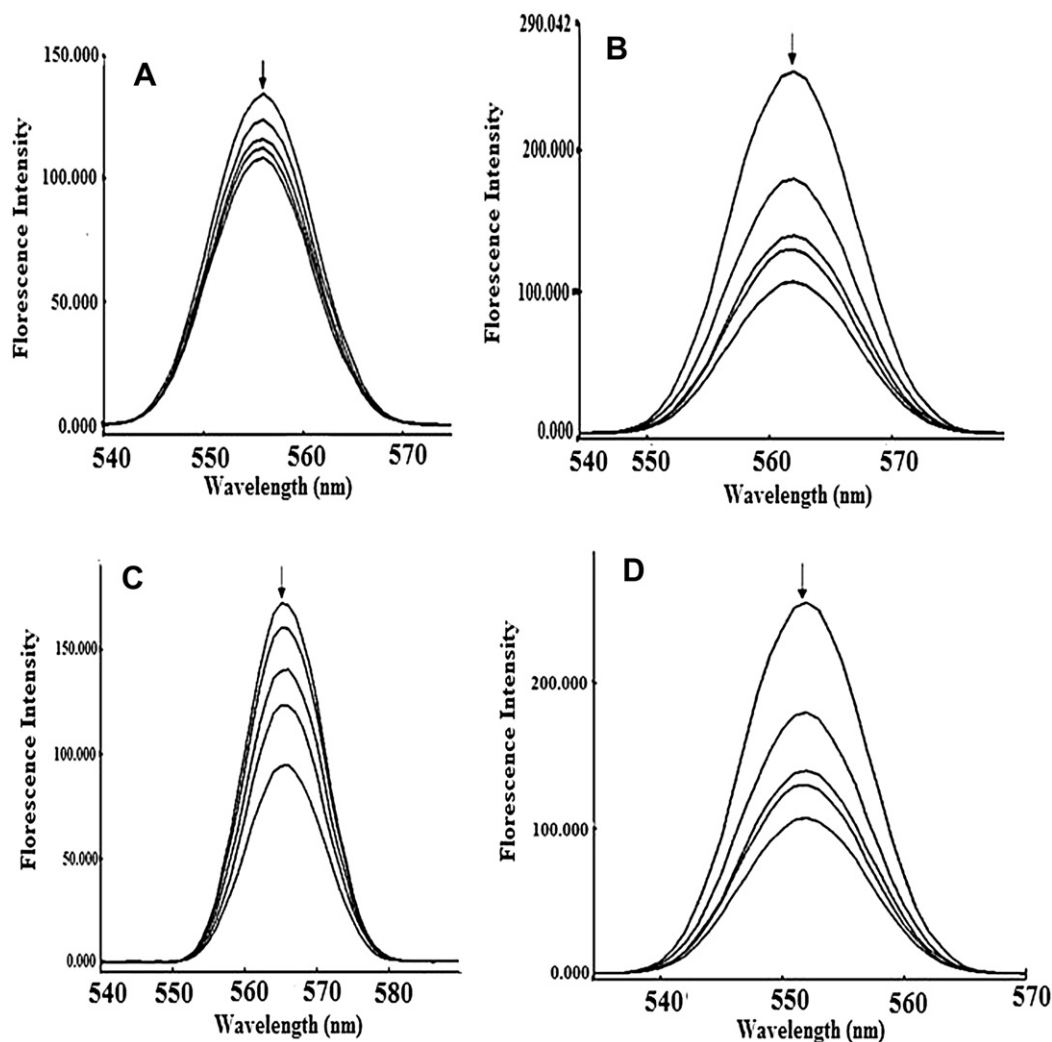


Fig. 8. Emission quenching spectra of [Cu(L)(OAc)(H₂O)₂](1); A, [Cu(L)(Phen)(OAc)](2); B, [Cu(L)(tpimH)(OAc)(H₂O)](3); C, [Cu(L)(tfbimH)(OAc)(H₂O)](4); D in presence of [CT-DNA] (1.89×10^{-5} M) with increasing concentration of quencher [Fe(CN)₆]⁴⁻ ($0-1.91 \times 10^{-4}$ M). Arrows show the intensity changes upon addition of the complexes (1×10^{-5} M).

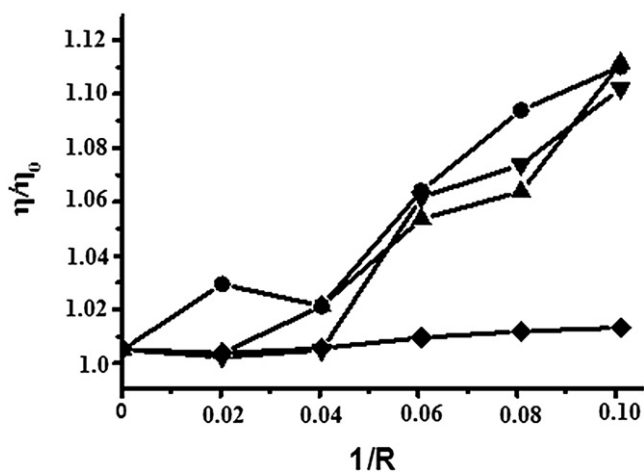


Fig. 9. Effect of increasing amount of complexes 1 (◆), 2 (▼), 3 (▲) and 4 (●) (prepared in MeOH) on the relative viscosities (η/η_0) of CT-DNA in Tris–HCl buffer (pH 7.2).

a supporting electrolyte (Fig. 10). The cyclic voltammograms of all the studied complexes exhibited lower peak current ratios (less than 1) attributed to quasi-reversible one electron redox process involving M^n/M^{n-1} couple. All the values corresponding to E_{PC} (V), E_{PA} (V), $E_{1/2}$ (V), ΔE_P and I_{PA}/I_{PC} are listed in Table 4. We also investigated the electrochemical responses of all the four complexes in presence of CT-DNA (Table 4B). A significant reduction in their respective peak potentials, cathodic and anodic peak currents can be attributed to slow diffusion of the equilibrium mixtures of these complexes (free and DNA bound) at the electrode surface [52]. The $E_{1/2}$ shifts these complexes towards lower negative potential confirms their binding to CT-DNA [56]. However, the positive shift in the E_{PC} or E_{PA} value is indicative of intercalation of the complex into the DNA double helix while negative shift reveals the involvement of electrostatic interactions [57].

5.5. SOD activity

The $O_2^{\cdot-}$ scavenging activity (IC_{50}) of the complexes [Cu(L-H)(OAc)(H₂O)₂], [Cu(LH)(phen)(OAc)], [Cu(LH)(tpimH)(OAc)(H₂O)] and [Cu(LH)(tfbimH)(OAc)(H₂O)] was determined by NBT assay using UV–vis spectroscopy. All Cu(II) complexes demonstrated SOD

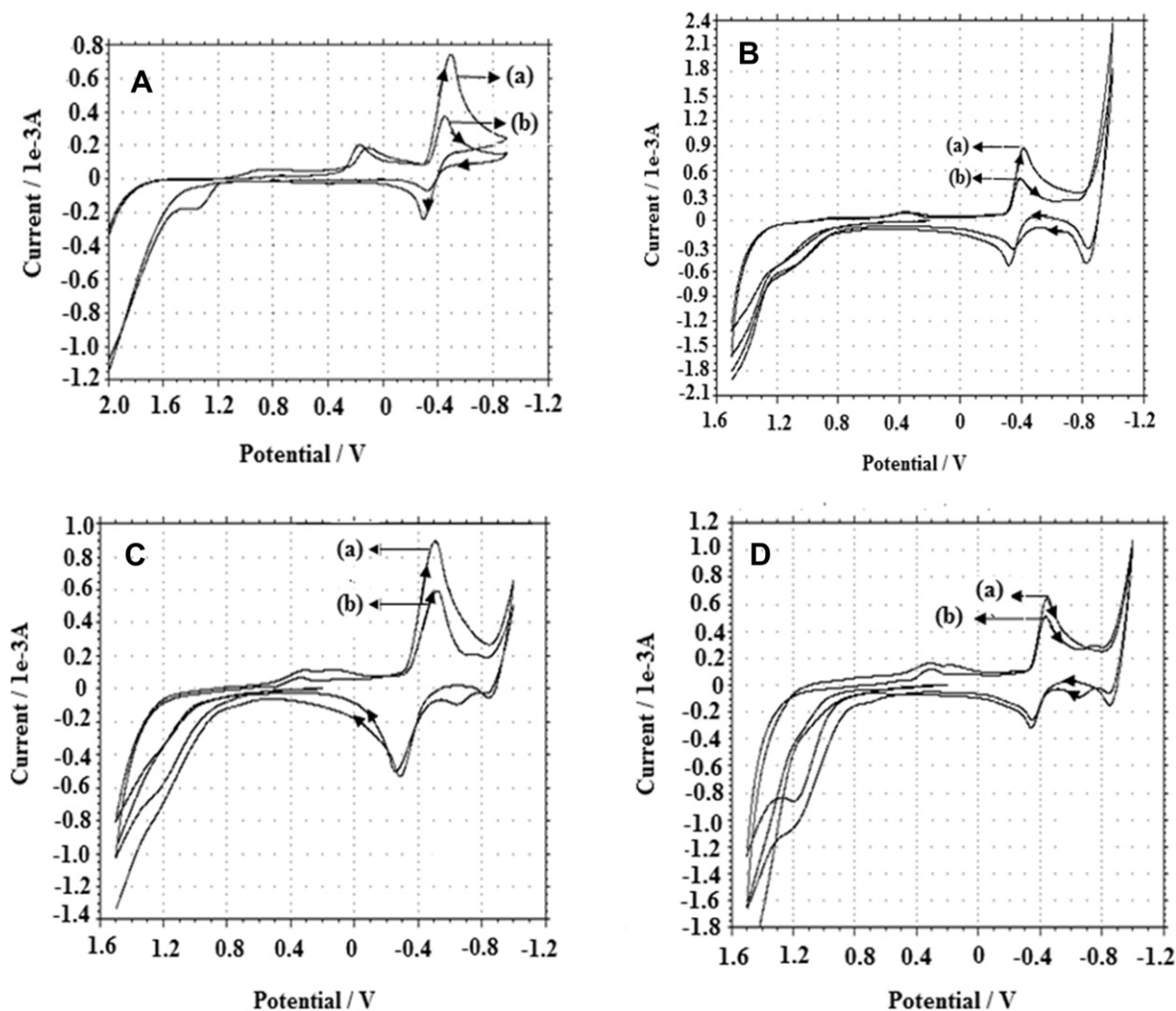


Fig. 10. Cyclic voltammogram (5:95 MeOH/H₂O, 25 °C) of [Cu(L)(OAc)(H₂O)₂](1); A, [Cu(L)(Phen)(OAc)](2); B, [Cu(L)(tpimH)(OAc)(H₂O)](3); C, [Cu(L)(tfbimH)(OAc)(H₂O)](4); D, at (a) unbound and (b) in presence of CT-DNA, [complex 1–4] = 1×10^{-3} M, [DNA] = 6×10^{-3} M.

activity in the micromolar range (IC_{50}) varying from 0.58 to 11.40 μ M as shown in Table 5. Complex [Cu(LH)(phen)(OAc)] possesses higher SOD mimetic activity among all the studied complexes. Although, the IC_{50} values of the Cu(II) complexes are higher than those reported for native bovine erythrocyte SOD (0.04 μ M), they are in good agreement with the IC_{50} values of previously reported synthetic SOD mimics [58,59].

Table 4

Cyclic voltammetric results of complexes [Cu(LH)(OAc)(H₂O)₂](1), [Cu(LH)(phen)(OAc)](2), [Cu(LH)(tpimH)(OAc)(H₂O)](3) and [Cu(LH)(tfbimH)(OAc)(H₂O)](4), (A) in the absence of CT-DNA, (B) in the presence of CT-DNA.

Complexes	E_{PC} (V)	E_{PA} (V)	$E_{1/2}$ (V)	ΔE_p	I_{PA}/I_{PC}
(A)					
1	-0.4896	-0.2963	-0.3929	0.1933	0.3150
2	-0.4167	-0.3212	-0.3689	0.0955	0.6030
3	-0.5049	-0.2842	-0.3945	0.2207	0.5880
4	-0.4459	-0.3432	-0.3945	0.1027	0.4632
(B)					
1	-0.4474	-0.3215	-0.3844	0.1259	0.1755
2	-0.3947	-0.3232	-0.3589	0.0515	0.6355
3	-0.5194	-0.2622	-0.3908	0.2572	0.8303
4	-0.4388	-0.3435	-0.3911	0.0885	0.4906

5.6. Gel electrophoresis studies

5.6.1. DNA cleavage demonstrating SOD mimetic activity

The higher SOD activity of complex [Cu(LH)(phen)(OAc)] as ascertained by NBT assay, was further confirmed by employing DNA cleavage studies. Our experiment is based on the mechanism of SOD activity of native bovine erythrocyte SOD (Cu/Zn), which converts the $O_2^{\cdot -}$ into H_2O_2 and O_2 . However, this H_2O_2 was further converted into H_2O by catalase. Native SOD, a homodimer metalloenzyme, undergoes glycation *in vivo* [60] resulting into the release of free Cu(II) ion, which further participates in the generation of OH^{\cdot} by Fenton-type reaction. To assess the DNA cleavage

Table 5

SOD activity profile of complexes [Cu(LH)(OAc)(H₂O)₂](1), [Cu(LH)(phen)(OAc)](2), [Cu(LH)(tpimH)(OAc)(H₂O)](3) and [Cu(LH)(tfbimH)(OAc)(H₂O)](4).

Complexes	Concentration ^a (μ M)
1	11.40 (± 0.08)
2	0.58 (± 0.06)
3	3.20 (± 0.04)
4	0.67 (± 0.06)

^a Equivalent to 1 U SOD (0.04 μ M).

ability of complex [Cu(LH)(phen)(OAc)] a fixed concentration (200 μ M) of the complex and pBR322 DNA was taken and incubated in a mixture (1:10) containing xanthine oxidase (prepared with 50 mM Tris–HCl, pH 8.0 sample buffer) and hypoxanthine (prepared in 50 mM Tris–HCl, pH 8.0 assay buffer + 0.1 mM diethylenetriaminepentaacetic acid (DTPA) + 0.1 mM hypoxanthine). Change in the electrophoretic mobility of plasmid DNA was observed on agarose gel. As depicted in Fig. 11 (lane L2), $O_2^{\cdot -}$ generated by the reaction of xanthine oxidase and hypoxanthine did not cause loss of the supercoiled form (SC form; Form I) [61]. In presence of native SOD, an inhibition of the cleavage was observed (Fig. 11, lane L3), which reveals that OH^{\cdot} is not generated due to the absence of glycation process in the experimental conditions. However, OH^{\cdot} is easily produced by mixing complex [Cu(LH)(phen)(OAc)] with $O_2^{\cdot -}$. As a consequence the supercoiled form (SC form; Form I) was converted into the nicked circular form (NC form; Form II) and linear circular form (LC form; Form III) (Fig. 11, lane L4) which confirms the involvement of complex [Cu(LH)(phen)(OAc)] in double strand DNA cleavage. Furthermore, the mixture containing complex [Cu(LH)(phen)(OAc)] and O_2 reveals minor conversion of Form I into the Form II as displayed in Fig. 11 (lane L5).

To further ascertain the role of OH^{\cdot} in the cleavage process, the electrophoretic pattern of plasmid pBR322 DNA was observed in the presence of radical scavenger DMSO (hydroxyl radical) and NaN_3 (singlet oxygen). Upon addition of DMSO to complex [Cu(LH)(phen)(OAc)] + $O_2^{\cdot -}$ system, inhibition of the cleavage was observed (Fig. 11, lane L6) suggestive of the involvement of freely diffusible OH^{\cdot} in the cleavage mechanism. However, no such quenching in the cleavage of the pBR322 DNA was observed in presence of NaN_3 revealing the non-participation of singlet oxygen in cleavage mechanism (Fig. 11, lane L7).

Besides, Form II was slightly inhibited in presence of catalase (Fig. 11, lane L8) which reveals slow catalyzation of H_2O_2 by the enzyme. Complex [Cu(LH)(phen)(OAc)], however undergoes rapid interaction with a major part of H_2O_2 as compared to catalase and generates OH^{\cdot} as ascertained by the conversion of Form I into Form II. These findings fulfil the prerequisite for complex [Cu(LH)(phen)(OAc)] to act as a potent SOD mimic.

5.6.2. DNA cleavage without added reductant

To assess the DNA cleavage ability of complex [Cu(LH)(phen)(OAc)] it was incubated with pBR322 DNA at different concentrations (25–200 μ M) in 15% H_2O_2 /0.01 mM HCl/10 mM NaCl buffer at pH 7.2 (Fig. 12) for 1 h. A concentration dependent DNA cleavage was observed after the reaction mixture was subjected to gel

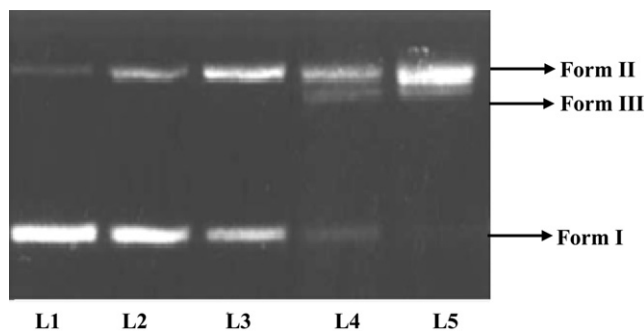


Fig. 12. Gel electrophoresis pattern showing cleavage of pBR322 supercoiled DNA (300 ng) by complex [Cu(L)(Phen)(OAc)]. Lane L1: DNA; lane L2: 25 μ M [Cu(L)(Phen)(OAc)] + DNA; lane L3: 50 μ M [Cu(L)(Phen)(OAc)] + DNA; lane L4: 150 μ M [Cu(L)(Phen)(OAc)] + DNA; lane L5: 200 μ M [Cu(L)(Phen)(OAc)] + DNA.

electrophoresis. The conversion of supercoiled (SC form; Form I) into the nicked circular form (NC form; Form II) was observed with the increase in concentration of complex [Cu(LH)(phen)(OAc)] from 25 to 50 μ M while the linear circular form (LC form; Form III) was observed at 150–200 μ M indicating that complex [Cu(LH)(phen)(OAc)] is involved in double strand DNA cleavage. These result confirms the efficient cleavage activity of complex [Cu(LH)(phen)(OAc)] which corroborates with the results of binding studies.

5.6.3. DNA cleavage with added reductant

Cleavage efficiency of Cu(II) complexes was also monitored in the presence of activators [62,63]. To examine whether reducing agents present in the reaction mixture could account for the higher rates of pBR322 DNA degradation by complex [Cu(LH)(phen)(OAc)] in 5 mM Tris–HCl/50 mM NaCl buffer at pH 7.2, cleavage reaction was performed in presence of various reducing agent viz., H_2O_2 , ascorbate (Asc), 3-mercaptopyruvic acid (MPA), and glutathione (GSH) (Fig. 13). In presence of H_2O_2 , a significant conversion of Form I into Form II was observed (Fig. 13, lane 4), as compared to other activators (Fig. 13, lane 2, 3 and 5). And follows the order $H_2O_2 > Asc = MPA > GSH$, which is similar to the nuclease activity of various mononuclear Cu(II) complexes [64,65].

5.6.4. DNA cleavage in the presence of recognition elements (groove binding)

In order to probe the potential interacting site of the complex [Cu(LH)(phen)(OAc)] with plasmid pBR322 DNA, the cleavage

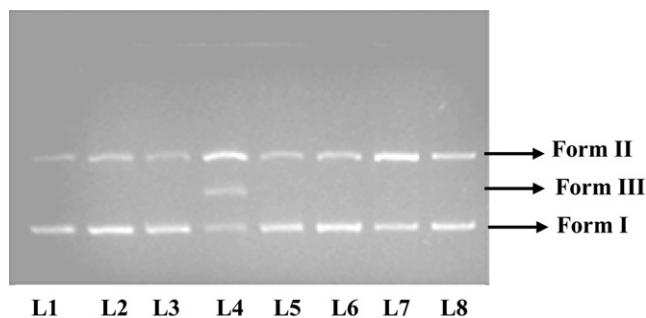


Fig. 11. Gel electrophoresis pattern showing cleavage of pBR322 supercoiled DNA (300 ng) by complex [Cu(L)(Phen)(OAc)](200 μ M). $O_2^{\cdot -}$ generated by incubation of XOD and hypoxanthine (1:10) as described in the experimental procedure. Lane L1: DNA; lane L2: $O_2^{\cdot -}$; lane L3: $O_2^{\cdot -}$ + SOD (15 units); lane L4: [Cu(L)(Phen)(OAc)] + $O_2^{\cdot -}$; lane L5: [Cu(L)(Phen)(OAc)] + O_2 ; lane L6: [Cu(L)(Phen)(OAc)] + $O_2^{\cdot -}$ + DMSO (400 μ M); lane L7: [Cu(L)(Phen)(OAc)] + $O_2^{\cdot -}$ + NaN_3 (400 μ M); lane L8: [Cu(L)(Phen)(OAc)] + $O_2^{\cdot -}$ + catalase (15 units).

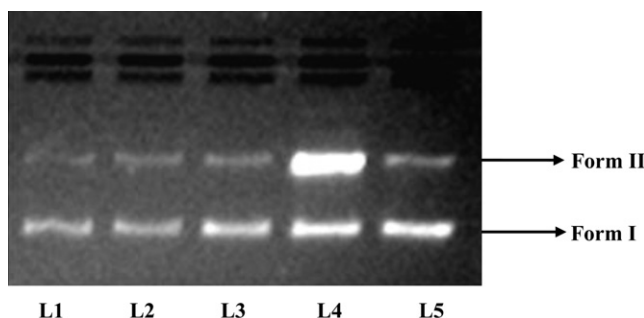


Fig. 13. Agarose gel electrophoresis showing the cleavage pattern of pBR322 plasmid DNA (300 ng) by complex [Cu(L)(Phen)(OAc)](200 μ M) in presence of different activating agent at 312 K after incubation for 30 min. Lane L1, DNA control; lane L2, DNA + [Cu(L)(Phen)(OAc)] + glutathione (400 μ M); lane L3, DNA + [Cu(L)(Phen)(OAc)] + MPA (400 μ M); lane L4, DNA + [Cu(L)(Phen)(OAc)] + H_2O_2 (400 μ M); lane L5, DNA + [Cu(L)(Phen)(OAc)] + Asc (400 μ M).

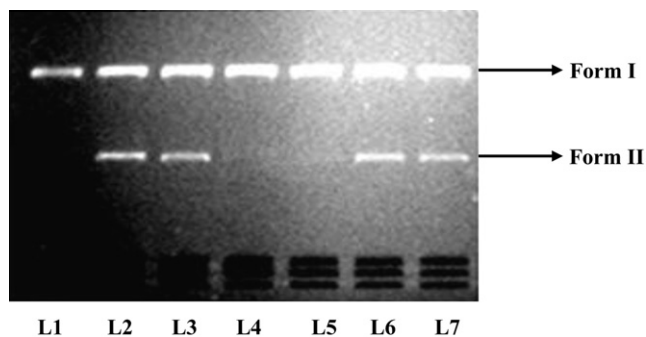


Fig. 14. Agarose gel electrophoresis pattern showing the cleavage of pBR322 plasmid DNA (300 ng) by complex $[\text{Cu}(\text{L})(\text{Phen})(\text{OAc})]$ (200 μM) in the presence of DNA minor binding agent DAPI, major binding agent MG and standard radical scavengers at 310 K after incubation for 30 min. Lane L1, DNA control; lane L2, DNA + $[\text{Cu}(\text{L})(\text{Phen})(\text{OAc})]$ + DAPI (8 μM); lane L3, DNA + $[\text{Cu}(\text{L})(\text{Phen})(\text{OAc})]$ + methyl green (2.5 μL of a 0.01 mg/ml solution); lane L4, DNA + $[\text{Cu}(\text{L})(\text{Phen})(\text{OAc})]$ + DMSO (400 μM); lane L5, DNA + $[\text{Cu}(\text{L})(\text{Phen})(\text{OAc})]$ + EtOH (400 μM); lane L6, DNA + $[\text{Cu}(\text{L})(\text{Phen})(\text{OAc})]$ + NaNa_3 (400 μM); lane L7, $[\text{Cu}(\text{L})(\text{Phen})(\text{OAc})]$ + SOD (15 units).

experiment was carried out in presence of minor groove binding agent, DAPI [66] and major groove binding agent, methyl green (MG) [67]. The results demonstrate that (Fig. 14, lane 2, 3) the DNA cleavage was neither affected by DAPI nor methyl green, implicating non affinity of the complex towards the DNA major/minor groove.

5.6.5. DNA cleavage in the presence of reactive oxygen species

To probe the DNA cleavage mechanism by complex $[\text{Cu}(\text{LH})(\text{phen})(\text{OAc})]$, some standard radical scavengers were used prior to the addition of complex $[\text{Cu}(\text{LH})(\text{phen})(\text{OAc})]$ to plasmid pBR322 DNA. The involvement of ROS in the cleavage mechanism was

investigated by studying comparative reactions in presence of various radical scavengers like DMSO, EtOH (hydroxyl radical), sodium azide (singlet oxygen) and SOD (superoxide). In presence of DMSO and EtOH (Fig. 14, lane 4, 5) inhibition of the cleavage was observed while the presence of sodium azide and superoxide dismutase did not affect the cleavage mechanism (Fig. 14, lane 6, 7). Thus, freely diffusible OH^\bullet is considered as the active species responsible for pBR322 DNA cleavage.

6. Antimicrobial screening

Furthermore, the complexes $[\text{Cu}(\text{LH})(\text{OAc})(\text{H}_2\text{O})_2]$, $[\text{Cu}(\text{LH})(\text{phen})(\text{OAc})]$, $[\text{Cu}(\text{LH})(\text{tpimH})(\text{OAc})(\text{H}_2\text{O})]$ and $[\text{Cu}(\text{LH})(\text{tfbimH})(\text{OAc})(\text{H}_2\text{O})]$ were screened for their antimicrobial activity against certain pathogenic bacterial and fungal species using agar well dilution method and the results of antimicrobial activities were summarized in Table 6. All the complexes were found to exhibit significant activity against Gram (+ve) and Gram (-ve) bacteria. We observed excellent activity of complex $[\text{Cu}(\text{LH})(\text{phen})(\text{OAc})]$ against *Candida albicans* and *Aspergillus niger*.

7. Antitumor activity

In vitro antitumor activity of complexes $[\text{Cu}(\text{LH})(\text{OAc})(\text{H}_2\text{O})_2]$, $[\text{Cu}(\text{LH})(\text{phen})(\text{OAc})]$ and $[\text{Cu}(\text{LH})(\text{tfbimH})(\text{OAc})(\text{H}_2\text{O})]$ was screened against 16 different human carcinoma cell lines of different histological origin; K562 (Leukaemia), ZR-75-1, MCF7, (Breast), Colo205, HT29, HCT15, SW620 (Colon), SiHa (Cervix), T24 (bladder), A498,786-O (kidney), MIAPACA2 (Pancreas), Hop-62 (Lung), PC3 (Prostrate), DWD (Oral) and A549 (Alveolar) and GI_{50} values were listed in Table 7. However it must be noted that the test stock solutions of the complexes 1–4 (1 mg/mL) were prepared by dissolving the substance in 100 μL of DMSO and completed with 900 μL of tissue culture medium. DMSO is

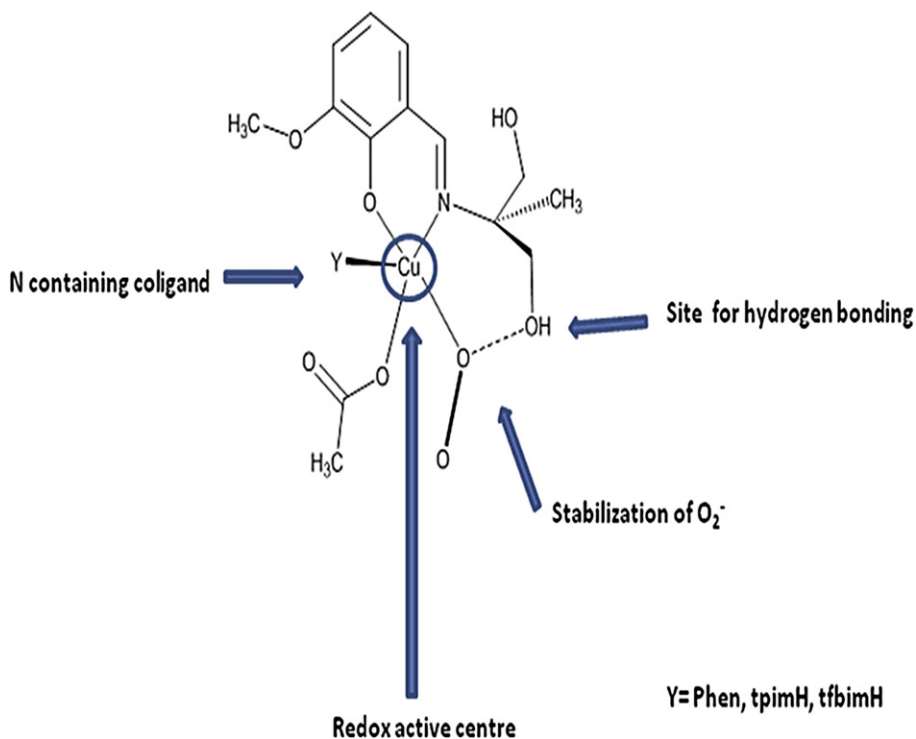


Chart 1. Synthetic model representing SOD mimic.

Table 6

Antimicrobial activity of complexes [Cu(LH)(OAc)(H₂O)₂](**1**), [Cu(LH)(phen)(OAc)](**2**), [Cu(LH)(tpimH)(OAc)(H₂O)](**3**) and [Cu(LH)(tfbimH)(OAc)(H₂O)](**4**) by agar well dilution method.

Cmp ^a	S. a ^b	B. s ^c	S. t ^d	E. c ^e	C. a ^f	A. n ^g
1	15	–	–	–	12	–
2	30	20	10	31	16	10
3	Under investigation					
4	18	–	–	11	13	–

^a Activity profile <11 mm, poor activity (+); <15 mm, moderate activity (++); <20 mm, very good activity (+++).

^b Complex (1 mg/mL).

^c *S. aureus* (SA-22).

^d *B. subtilis* (MTCC 121).

^e *S. typhimurium* (MTCC 98).

^f *E. coli* (K-12).

^g *C. albicans* (Clinical isolate).

^h *A. niger* (Clinical isolate).

a biocompatible solvent used in several biological test at lower concentration. Afterwards, the tested complexes were further diluted in culture medium to reach the final concentrations of 10, 20, 40 and 80 ng/μL, respectively. Now, test were performed in triplicates with each well receiving 900 μL of cell suspension and 10 μL of the drug solution. But if higher concentration of the solvent is used it does not reveal any cytotoxicity [68]. The results of antitumor activity of the studied complexes show the negligible effect of DMSO in the complex solutions at a given range of concentrations. The result showed excellent potential of complex [Cu(LH)(phen)(OAc)] towards 14 different human carcinoma cell lines viz., K562 (Leukaemia), MCF7, (Breast), HT29, HCT15, SW620 (Colon), SiHa (Cervix), T24 (bladder), A498,786-O (kidney), MIA-PACA2 (Pancreas), Hop-62 (Lung), PC3 (Prostrate), DWD (Oral) and A549 (Alveolar) with a GI₅₀ value comparable with the values obtained for standard drug Adriamycin (ADR), which is taken as positive control while complexes [Cu(LH)(OAc)(H₂O)₂] and [Cu(LH)(tfbimH)(OAc)(H₂O)] were found active towards 786-O (kidney) cell line. Further *in vivo* investigations are in progress in order to understand the mechanism of the antiproliferative activity for these complexes.

8. Conclusion

Synthesis and characterization of four Cu(II) *o*-vanillin Schiff base complexes [Cu(LH)(OAc)(H₂O)₂], [Cu(LH)(phen)(OAc)], [Cu(LH)(tpimH)(OAc)(H₂O)] and [Cu(LH)(tfbimH)(OAc)(H₂O)] were carried out using different coligands viz., phen, tpimH and tfbimH. The effect of varying coligands on the DNA binding and other biological activities: SOD mimetic, antimicrobial and antitumor were studied in detail. The results of electronic absorption titrations, fluorescence, viscosity and cyclic voltammetry studies of Cu(II) complexes carried out using CT-DNA indicated the non-covalent mode of binding of these complexes with CT-DNA i.e. electrostatic interactions for complex **1** and intercalation for complex **2–4**.

Table 7

Cytotoxicity against different tumor cell lines in terms of GI₅₀ (μg/ml) value.

Cmp	K562	Zr-75-1	Colo205	MCF7	SiHa	T24	A498	MIA-PACA2	Hop-62	PC3	HT29	HCT15	DWD	A549	SW620	786-O
1	41.7	>80	61.0	29.4	28.6	37.9	49.5	31.2	55.5	23.8	35.4	29.3	47.1	36.0	42.4	6.9
2	<10	33.3	26.9	<10	<10	<10	<10	<10	<10	<10	<10	10.2	<10	<10	<10	<10
3	Under investigation															
4	39.1	71.4	44.1	27.3	27.5	39.1	38.0	32.0	55.8	24.1	33.7	31.3	33.7	32.9	42.7	10.0
ADR ^a	<10	<10	<10	<10	<10	<10	<10	<10	<10	<10	<10	<10	<10	<10	<10	<10

^a GI₅₀ ≤ 10 is considered to demonstrate activity.

^b Adriamycin (taken as positive control).

Quenching experiments were performed using [Fe(CN)₆]⁴⁻ which reveal the binding strength of complexes with CT-DNA. The quenching efficiency is evaluated by using Stern–Volmer constant K_{SV} which follows the same order of binding affinity of complexes towards CT-DNA as observed for K_b : [Cu(LH)(tfbimH)(OAc)(H₂O)] > [Cu(LH)(tpimH)(OAc)(H₂O)] > [Cu(LH)(phen)(OAc)] > [Cu(LH)(OAc)(H₂O)₂]. SOD activity of complex **2** was measured by employing NBT assay that showed excellent IC₅₀ value of 0.58 (±0.06) μM for the complex. Gel electrophoretic pattern of complex **2** displayed remarkable double strand scission of pBR322 DNA via oxidative pathway. Also, SOD activity of complex **2** was analyzed by gel electrophoresis and is consistent with the participation of OH[•] in the cleavage process. *In vitro* antitumor activity results reveal excellent potential of complex **2** towards 14 different human carcinoma cell lines of different histological origin. The GI₅₀ values of complex **2** are comparable to those obtained for standard drug Adriamycin (ADR) while complex **1** and **4** were showed activity towards 786-O kidney cell line.

9. Experimental section

9.1. Materials

All the solvents used were of analytical grade and used as received (Sigma–Aldrich). Analytical grade reagents *o*-vanillin, 2-amino-2-methylpropane-1,3-diol, 1,10-phenanthroline (phen), 2,4,5-triphenylimidazole (tpimH), 2-trifluoromethyl-benzimidazole (tfbimH), Cu(OAc)₂·H₂O (Sigma Aldrich, Steinheim, Germany) were used as received. SOD activity was determined by using superoxide dismutase activity kit II Cat.No. 574601 (Calbiochem) according to the manufacturer's protocol. The kit utilizes a tetrazolium salt for the detection of superoxide radicals generated by xanthine oxidase and hypoxanthine. The supercoiled pBR322 DNA was purchased from Genei, Bangalore (India). Calf thymus DNA (CT-DNA) was purchased from Sigma–Aldrich. Deionized water was prepared with Bhanu Scientific Instruments co., Bangalore and is used for the preparation of the Tris–HCl buffer.

9.2. Synthesis

9.2.1. Synthesis of the proligand 2-((E)-(1,3-dihydroxy-2-methylpropan-2-ylimino)methyl)-6-methoxyphenol (LH)

The proligand LH was synthesized from the reaction of *o*-vanillin (100 mg, 0.65 mmol) and 2-amino-2-methylpropane-1,3-diol (70 mg, 0.65 mmol) according to the procedure reported earlier [69].

Yield: 82% (0.012 g, 0.53 mmol). M.p. 165 °C. Anal. (%) Calcd. for C₁₂H₁₇NO₄: C, 60.24; H, 7.16; N, 5.85. Found: C, 60.33; H, 7.24; N, 5.92. FT-IR (cm⁻¹): 3177s br ν(OH), 1637s ν(C=N of imine), 1494s, 1442s, 1393w, 1369m, 1339m, 1284w, 1216vs, 1160s, 1063vs, 956w, 925s, 888w, 850m, 793w, 746s, 720s ν(C=O + C=C). UV–visible [MeOH, λ_{max}/nm (ε/M⁻¹ cm⁻¹): 216 (46,296), 265 (37,735), 348 (28,735), 417sh (23,980). ESI-MS (MeCN) (+) (*m/z*, relative intensity

); 240 (100) [C₁₂H₁₇NO₄ + H]⁺. ¹H NMR (400 MHz, CDCl₃): δ, 14.4 (s br, 1H, Ph–OH), 8.43 (s, 1H, N=CH_{imine}), 6.89 (d, 2H, CH_{Ph}), 6.74 (t, 1H, CH_{Ph}), 3.88–3.80 (m, 4H, CH₂OH), 3.70 (s, 3H, OCH₃), 3.5 (s br, 2H, CH₂OH), 1.32 (s, 3H, CCH₃). ¹³C NMR (100 MHz, CDCl₃): δ, 163.9 (N=CH_{imine}), 129.2, 126.7, 123.7, 117.1, 114.4, 113.5 (C_{aromatics}), 68.2, 67.1 (CH₂OH), 64.0 (*tert*-C), 56.2 (OCH₃).

9.2.2. Synthesis of [Cu(LH)(OAc)(H₂O)₂] (1)

To a methanolic solution (10 mL) of the Schiff base ligand LH (0.5 g, 2.08 mmol) was added a solution of Cu(OAc)₂·H₂O (0.379 g, 2.089 mmol) in methanol (5 mL). The mixture was allowed to reflux at 60 °C for 1 h to ensure completion of reaction. The reaction mixture yielded a solid product (green coloured) which was isolated, washed with hexane and dried in vacuo.

Yield: 80% (0.663 g, 1.671 mmol). M.p. 127 °C. Anal. (%) Calcd. for C₁₄H₂₃CuNO₈: C, 42.37; H, 5.84; N, 3.53. Found: C, 42.50; H, 5.95; N, 3.59. FT-IR (cm⁻¹): 3234 ν(OH), 1621 ν(HC=N of imine), 1602 ν_{as}(COO), 1401 ν_s(COO), 466 ν(Cu–N), 528 ν(Cu–O). μ_{eff} (298 K): 1.88 BM. UV–visible [MeOH, λ_{max}/nm (ε/M⁻¹ cm⁻¹): 231 (43,290), 278 (35,866), 368 (27,106), 675 (14,814). λ_M (MeOH, 10⁻³ M) = 8.6 S cm² mol⁻¹. ESI-MS (MeCN) (+) (*m/z*, relative intensity %): 399 (20) [CuC₁₂H₁₇NO₄(CH₃COO)(H₂O)₂ + 4H⁺], 383.3 (80) [CuC₁₂H₁₇NO₄(CH₃COO)(H₂O) + 4H⁺], 319.4 (15) [CuC₁₂H₁₇NO₄(H₂O)]⁺, 301.4 (50) [CuC₁₂H₁₇NO₄]⁺, 304.6 (100) [CuC₁₂H₁₇NO₄ + 3H]⁺. TGA-DTA (mg % vs. °C): heating from 30 to 600 °C with a speed of 10 °C/min; from 80 to 100 °C loss of two water molecules (weight loss found 9.4%, calcd. 9.0%, Δ*H* = 13.3 kJ/mol), melting at 127 °C, exothermal event with an onset at 264 °C (Δ*H* = -7.9 kJ/mol), then progressive decomposition till 600 °C, with residue of 20.3% weight corresponding to CuO (calcd. 20.0%).

9.2.3. Synthesis of [Cu(LH)(phen)(OAc)] (2)

To a methanolic solution (5 mL) of complex 1 (0.5 g, 1.259 mmol) was added dropwise methanolic solution (5 mL) of phen (0.250 g, 1.26 mmol) and the reaction mixture was refluxed at 60 °C for 5 h. The reaction mixture yielded a solid product (green coloured) which was isolated, washed with diethyl ether and methanol in portion and dried in vacuum.

Yield: 82% (0.559 g, 1.03 mmol). M.p. 147 °C. Anal. (%) Calcd. for C₂₆H₂₇CuN₃O₆: C, 57.72; H, 5.03; N, 7.77. Found: C, 57.89; H, 5.12; N, 7.82. FT-IR (cm⁻¹): 3234 ν(H₂O + OH), 1625 ν(HC=N of imine), 1601 ν_{as}(COO), 1374 ν_s(COO), 1516 ν(C=N), 1429 ν(C=C), 536 ν(Cu–O), 472 ν(Cu–N). μ_{eff} (298 K): 1.95 BM. UV–visible [MeOH, λ_{max}/nm (ε/M⁻¹ cm⁻¹): 218 (45,806), 273 (36,541), 381 (26,246), 633 (15,797). λ_M (MeOH, 10⁻³ M) = 5.8 S cm² mol⁻¹. ESI-MS (MeCN) (+) (*m/z*, relative intensity %): 481 (100) [CuC₁₂H₁₇NO₄(phen)]⁺, 302.4 (65) [CuC₁₂H₁₇NO₄ + 2H]⁺. TGA-DTA (mg % vs. °C): heating from 30 to 600 °C with a speed of 10 °C/min; melting at 147 °C, exothermal event with an onset at 269 °C (Δ*H* = -5.3 kJ/mol), then progressive decomposition until to 600 °C, with residue of 15.2% weight corresponding to CuO (calcd. 14.7%).

9.2.4. Synthesis of [Cu(LH)(tpimH)(OAc)(H₂O)] (3)

This complex was synthesized according to the procedure described for complex 2 by using complex 1 (500 mg, 1.26 mmol) with tpimH (0.373 g, 1.26 mmol).

Yield: 72% (0.613 g, 0.72 mmol). M.p. >300 °C. Anal. (%) Calcd. for C₃₅H₃₇CuN₃O₇: C, 62.26; H, 5.52; N, 6.22. Found: C, 62.38; H, 5.61; N, 6.39. FT-IR (cm⁻¹): 3234 ν(H₂O + OH), 3202 ν(N–H), 1624 ν(HC=N of imine), 1602 ν_{as}(COO), 1315 ν_s(COO), 1544 ν(C=N), 1469 ν(C=C), 468 ν(Cu–N), 530 ν(Cu–O). μ_{eff} (298 K): 1.97 μ_B. UV–visible [MeOH, λ_{max}/nm (ε/M⁻¹ cm⁻¹): 202 (49,504), 229 (43,668), 278 (35,971), 372 (26,881), 650 (15,384). λ_M (MeOH, 10⁻³ M) = 9.9 S cm² mol⁻¹. ESI-MS (MeCN) (+) (*m/z*, relative intensity %): 676 (15) [C₁₂H₁₇CuNO₄(tpimH)(CH₃COO)(H₂O) + 2H⁺], 338 (100) [C₁₂H₁₇CuNO₄ + 2H₂O

+ H]⁺. TGA-DTA (mg % vs. °C): heating from 30 to 600 °C with a speed of 10 °C/min; from 80 to 100 °C loss of one water molecule (weight loss found 3.1%, calcd. 2.7%), exothermal event with an onset at 182 °C (Δ*H* = -6.7 kJ/mol), then progressive decomposition until to 600 °C, with residue of 12.2% weight corresponding to CuO (calcd. 11.8%).

9.2.5. Synthesis of [Cu(LH)(tfbimH)(OAc)(H₂O)] (4)

This complex was synthesized according to the procedure described for complex 2 by using complex 1 (500 mg, 1.26 mmol) with tfbimH (0.234 g, 1.26 mmol).

Yield: 80% (0.569 g, 1.007 mmol). M.p. 158 °C. Anal. (%) Calcd. for C₂₂H₂₆CuF₃N₃O₇: C, 46.77; H, 4.64; N, 7.44. Found: C, 46.82; H, 4.66; N, 7.48. FT-IR (cm⁻¹): 1626 ν(HC=N of imine), 1602 ν_{as}(COO), 1316 ν_s(COO), 1545 ν(C=N), 1469 ν(C=C), 3213 ν(N–H), 1128 ν(C–F), 465 ν(Cu–N), 560 ν(Cu–O). μ_{eff} (298 K): 1.99 BM. UV–visible [MeOH, λ_{max}/nm (ε/M⁻¹ cm⁻¹): 205 (48,780), 223 (44,843), 277 (36,101), 371 (26,954), 643 (15,552). λ_M (MeOH, 10⁻³ M) = 8.0 S cm² mol⁻¹. ESI-MS (MeCN) (+) (*m/z*, relative intensity %): 525 (20) [Cu(L)(tfbimH)(H₂O)₂ – H]⁺, 491 (25) [Cu(L)(tfbimH) + 3H]⁺, 304 (15) [Cu(L) + 2H]⁺. TGA-DTA (mg % vs. °C): heating from 30 to 600 °C with a speed of 10 °C/min; from 100 to 150 °C loss of one water molecule (weight loss found 3.4%, calcd. 3.2%), melting at 158 °C, then progressive decomposition until to 600 °C, with residue of 14.5% weight corresponding to CuO (calcd. 14.1%).

9.3. Methods

9.3.1. Physical measurements

Elemental analyses were carried out with a Fison instrument 1108 CHNS–O elemental analyzer. Melting points were obtained using SMP3 stuart scientific melting point apparatus. IR reflectance spectra were recorded from 4000 to 380 cm⁻¹ with a Perkin–Elmer Spectrum 100 FT-IR instrument. Molar conductance measurements were measured at room temperature on a Digsun Electronic conductivity Bridge. ¹H and ¹³C {¹H} NMR spectra were recorded on a 400 Mercury Plus instrument operating at room temperature (400 MHz for ¹H, 100 MHz for ¹³C) and with a Varian (200 MHz for ¹H, 50 MHz for ¹³C). TGA spectra were obtained with a STA 6000 Simultaneous Thermal Analyzer Perkin–Elmer by conducting the thermal studies under an inert atmosphere of dry nitrogen. Electron paramagnetic resonance (EPR) spectra of the Cu(II) complexes were obtained on a Varian E 112 EPR spectrometer at a frequency of 9.1 GHz under the magnetic field strength 3000 ± 1000 Gauss using tetracyanoethylene (TCNE) as field marker at LNT. H and C chemical shifts (δ) are reported in parts per million (ppm) from SiMe₄ (¹H and ¹³C calibration by internal deuterium solvent lock). Peak multiplicities are abbreviated: singlet, s; doublet, d; triplet, t; quartet, q; multiplet, m.

Absorption spectral titration experiments were performed with UV-1700 PharmaSpec UV–visible spectrophotometer (Shimadzu) spectrophotometer. UV–visible data were reported as λ_{max}/nm. Emission intensity measurements were carried out using Shimadzu RF-5301PC spectrofluorophotometer at room temperature. DNA binding experiments including absorption spectral traces, emission spectroscopy viscosity and cyclic voltammetry were performed in accordance with the standard methods and practices previously adopted by our laboratory [70]. A solution of calf thymus DNA in the Tris-hydroxymethylaminomethane buffer gave a ratio of UV absorbance at 260 and 280 nm of about 1.90 indicating that the DNA was sufficiently free of protein [71]. The DNA concentration per nucleotide was determined by absorption spectroscopy using the molar absorption coefficient (6600 M⁻¹ cm⁻¹) at 260 nm [72]. Magnetic susceptibilities were determined at 297 K with Sherwood scientific magnetic susceptibility balance. Diamagnetic corrections were carried out with Pascal's increments [73]. Cyclic voltammetry

measurements were carried out using a CH Instrument Electrochemical analyzer in a single compartmental cell. A conventional three electrode arrangement consisting of platinum wire as auxiliary electrode, glassy-carbon as working electrode and Ag(s)/AgCl electrode as reference electrode, was used in the presence of 0.4 M KNO₃ as supporting.

9.3.2. X-ray powder diffraction analysis

A strictly monophasic sample of the proligand LH was gently grinded in an agate mortar, and then deposited in the cavity of a 0.2 mm deep aluminium sample holder, equipped with a quartz monocrystal zero background plate (supplied by The Gem Dugout, State College, PA). Diffraction data were collected in the 5–105° 2θ range, sampling at 0.02°, on a θ:θ vertical scan Bruker AXS D8 Advance diffractometer, equipped with a linear Lynxeye position sensitive detector, set at 300 mm from the sample. Ni-filtered Cu-Kα_{1,2} radiation, λ = 1.5418 Å. Standard peak search methods, followed by indexing by TOPAS-R (V 3.0, 2005, Bruker AXS, Karlsruhe, Germany), allowed the determination of approximate cell parameters (GOF(26) = 17.5, space group P – 1, later confirmed by successful structure solution and refinement). Structure solution was initiated by employing a semirigid molecular fragment, flexible about a few torsional angles, build by molecular modelling and optimized by molecular mechanics (in vacuo) using the freeware programs distributed by ACD package (ChemSketch version 11.01, 2007). Simulated annealing allowed the location, orientation and conformation of the molecule, later refined by the Rietveld method. The fundamental parameter approach in describing the peak shapes was employed, the background contribution was modelled by a polynomial fit, and preferred orientation effects corrected by the March–Dollase formalism (001 pole, g = 0.91) A single isotropic thermal parameter was adopted for all atoms. Fig. 1 shows the final Rietveld refinement plots.

9.3.3. Crystal data for LH

LH: C₁₂H₁₇NO₄, fw = 239.27 g mol⁻¹; triclinic, P – 1, a = 7.2777(3) Å, b = 8.1109(2) Å, c = 10.6231(3) Å; α = 88.380(2)°, β = 87.383(2)°, γ = 102.853(2)°; V = 610.24(3) Å³; Z = 2; ρ_{calc} = 1.302 g cm⁻³; F(000) = 256; μ(Cu-Kα) = 8.17 cm⁻¹. R_p, R_{wp}, and R_{Bragg}, 0.045, 0.063 and 0.037, respectively for 38 parameters. The CIF file is supplied in the (Electronic Supporting Information) CCDC No. 829822.

9.3.4. Absorption titration of Cu(II) complexes binding to DNA

The binding strength of all the studied complexes with CT-DNA was determined by intrinsic binding constant K_b employing equation (1) and monitoring the changes in the absorbance of the π–π* and LMCT bands with increasing concentration of CT-DNA.

$$[\text{DNA}]/\varepsilon_a - \varepsilon_f = [\text{DNA}]/\varepsilon_b - \varepsilon_f + 1/K_b(\varepsilon_b - \varepsilon_f) \quad (1)$$

Where ε_a, ε_f and ε_b corresponds to (A_{obsd}/[Cu]), the extinction coefficient of free Cu(II) complex and the extinction coefficient for the Cu(II) complex in the fully bound forms, respectively. A plot of [DNA]/ε_a – ε_f vs [DNA], where [DNA] is the concentration of DNA in the base pair, gives K_b as the ratio of slope to the intercept.

9.3.5. DNA strand break analysis

The pBR322 DNA in 50 mM Tris–HCl, pH 8.0, containing 0.1 mM DTPA was incubated with complex [Cu(LH)(phen)(OAc)] which exhibit higher SOD activity among complexes 1–4. O₂^{•-} was generated from XOD and hypoxanthine for 1 h. The samples were analyzed by electrophoresis at 100 V in 0.7% agarose gel in Tris acetate EDTA buffer at 25 °C by adding 4 μL volume of loading

buffer. The gels were stained with ethidium bromide (EB) and visualized under ultraviolet light.

9.3.6. Measurement of SOD-like activity

Superoxide dismutase (SOD)-like activity was investigated using Beauchamp and Fridovich's method – as improved by Imanari et al. [74]. This method is based on the inhibitory effect of SOD on the reduction of nitrobluetetrazolium (NBT) by the O₂^{•-} generated by the xanthine/xanthine oxidase system. The assay was carried out in the assay buffer containing 50 mM Tris HCl, pH 8.0, 0.1 mM DTPA and 0.1 mM hypoxanthine. Radical detector consists of a tetrazolium salt and is diluted by assay buffer. Similarly, the solutions of SOD standards and xanthine oxidase were prepared in sample buffer consisting of 50 mM Tris–HCl, pH 8.0. All the studied complexes were dissolved in ethanol and absorbance was reported for each set of concentrations after 15 min interval. Results were graphed as % inhibition of NBT reduction taken at various concentrations (0 μM–20 μM) for each of the studied complexes. IC₅₀ values are reported equivalent concentrations (μM) to 1U bovine erythrocyte superoxide dismutase (native SOD).

9.3.7. Antimicrobial activity

9.3.7.1. Antifungal screening. All the studied complexes were tested for their *in vitro* growth inhibition activity against pathogenic fungus viz., *C. albicans* and *A. niger* cultured on potato dextrose agar (PDA) medium and incubated at 25 ± 2 for 72 h by using poison food technique [75]. The PDA medium was sterilized in autoclave in 15 kg/cm² at 121 °C which keeps the medium to retain its normal temperature. Solutions of each of the complex was added in the PDA medium at different concentrations in the range of (10–50) × 10⁻⁶ M. The inhibition of the fungal growth, expressed as percent, was determined on the growth in test plates compared to respective control plates (untreated), as given by Vincent equation (2) [76].

$$\text{Inhibition \%} = (C - T)/C \times 100 \quad (2)$$

Where C is the diameter of fungal growth of the control plate and T is the diameter of the fungal on the test plate.

9.3.7.2. Antibacterial screening. Solutions of the studied complexes (10–50) × 10⁻⁶ M in DMSO were applied on a paper disc prepared from sterilized paper (3 mm diameter) with a micropipette. The discs were left in an incubator for 30 h at 37 °C and then applied on the bacterial growth viz., *Staphylococcus aureus*, *Bacillus subtilis*, *Salmonella typhimurium* and *Escherichia coli* on potato dextrose agar (PDA) plates. Minimal agar was used for growth of specific bacterial species. Agar (50 g) was suspended in freshly distilled water (1 L), allowed to soak for 15 min and then boiled on water bath until the agar was completely dissolved. The mixture was autoclaved for 15 min at 120 °C and then poured into previously washed and sterilized petri dishes and stored at 40 °C for inoculation.

9.3.8. Antitumor activity

The cell lines used for *in vitro* antitumor screening activity were, K562, ZR-75-1, Colo205, MCF7, SiHa, T24, A498, MIAPACA2, Hop-62, PC3, HT29, HCT15, DWD, A549, SW620 and 786-O. These human cancer cell lines were procured and grown in RPMI-1640 medium supplemented with 10% foetal bovine serum (FBS) and antibiotics to study growth pattern of these cells. The proliferation of the cells upon treatment with the studied complexes was determined using the sulphorhodamine-B (SRB) semi automated assay. Cells were seeded in 96 well plates at an appropriate cell density to give optical density in the linear range (from 0.5 to 1.8) and were incubated at 37 °C in CO₂ incubator for 24 h. Stock solutions of the studied

complexes were prepared in DMSO (100 μ L) and further diluted to 10 μ L, 20 μ L, 40 μ L, 80 μ L, respectively. Tests were performed in triplicates with each well receiving 900 μ L of cell suspension and 10 μ L of the drug solution. Appropriate positive control (Adriamycin) and vehicle controls were also run. The plates with cells were incubated in CO₂ incubator with 5% CO₂ for 24 h followed by drug addition. The plates were incubated further for 48 h. Termination of experiment was done by gently layering the cells with 50 μ L of chilled 30% TCA (in case of adherent cells) and 50% TCA (in case of suspension cultures) for cell fixation and kept at 4 °C for 1 h. Plates were washed, air-dried and stained with 50 μ L of 0.4% SRB in 1% acetic acid for 20 min. The bound SRB was eluted by adding 100 μ L 10 mM Tris (pH 10.5) to each of the wells. The absorbance was read at 540 nm with 690 nm as reference wavelength. All experiments were repeated three times. The values of GI₅₀, the drug concentration resulting in a 50% reduction in the net protein increase, were calculated for all cells treated following the equation (3).

$$(\text{Growth inhibition of } 50\%)GI_{50} = [(T_i - T_z) / (C - T_z)] \times 100 = 50 \quad (3)$$

Where T_z , C and T_i corresponds to time zero, control growth, and test growth in the presence of drug at the various concentration levels [77].

Acknowledgements

We thank, University of Camerino, Italy, for providing financial support with useful suggestions throughout this work and facilitating NMR, elemental analysis, magnetic susceptibility and IR facility, Department of Biotechnology, New Delhi for generous financial support (Scheme No. BT/PR6345/Med/14/784/2005), RSIC, Punjab University, Chandigarh for spectroscopy facility, Dr. Iqbal Ahmad, Interdisciplinary agricultural microbiology, Aligarh Muslim university, for antimicrobial analysis and Dr. (Mrs.) Aarti Juvekar, (ACTREC), Kharghar, Navi Mumbai, for assessing cellular proliferation through (SRB) assay against 16 different human carcinoma cell lines.

References

- (a) T.W. Hambley, *Science* 318 (2007) 1392;
(b) H. Sigel, *Metal Ions in Biological Systems*, vol. II, M. Dekker, Inc. New York, 1980;
(c) B.K. Kepler, *Metal Complexes in Cancer Chemotherapy*, VCH, Weinheim, 1993;
(d) Z. Guo, P.J. Sadler, *Angew. Chem. Int. Ed. Engl.* 38 (1999) 1512;
(e) M. Gielen, E.R.T. Tiekink, *Metallotherapeutic Drugs and Metal-Based Diagnostic Agents, the Use of Metals in Medicine*, Wiley, Chichester, 2005;
(f) C.X. Zhang, S.J. Lippard, *Curr. Opin. Chem. Biol.* 7 (2003) 481;
(g) J.L. Sessler, S.R. Doctrow, T.J. McMurry, S.J. Lippard, *Medicinal Inorganic Chemistry*, ACS, Washington, D.C., 2003.
- C. Marzano, M. Pellei, F. Tisato, C. Santini, *Anti-Cancer Agents Med. Chem.* 9 (2009) 185.
- (a) J.R. Turnlund, W.R. Keyes, H.L. Anderson, L.L. Acord, *Am. J. Clin. Nutr.* 49 (1989) 870;
(b) R.N. Patel, N. Singh, K.K. Shukla, V.L.N. Gundla, U.K. Chauhan, *Spectrochim. Acta A: Mol. Biomol. Spectrosc.* 63 (2006) 21;
(c) J.R.J. Sorenson, *Prog. Med. Chem.* 26 (1989) 437.
- A. De Vizcaya-Ruiz, A. Rivero-Muller, L. Ruiz-Ramirez, G.E. Kass, L.R. Kelland, R.M. Orr, et al., *Toxicol In Vitro.* 14 (2000) 1.
- I. Gracia-Mora, L. Ruiz-Ramirez, C. Gomez-Ruiz, M. Tinoco-Mendez, A. Marquez-Quinones, L. Romero de Lira, et al., *Met.-Based Drug* 8 (2001) 19.
- T. Yoshikawa, S. Kokura, K. Tainaka, K. Itani, H. Oyamada, T. Kaneko, Y. Naito, M. Kondo, *Cancer Res.* 53 (1993) 2326.
- D.C. Wallace, *Science* 283 (1999) 1482.
- E. Ueta, K. Yoneda, T. Yamamoto, *Jpn. J. Cancer Res.* 90 (1999) 555.
- Y. Kobayashi, K. Kariya, K. Saigenji, K. Nakamura, *Cancer Biother.* 9 (1994) 171.
- X.-M. Yin, Z. Dong, *Essentials of Apoptosis, a Guide for Basic and Clinical Research*, Totowa, New Jersey (2003).
- (a) G. Kolks, C.R. Frihart, H.N. Rabinowitz, S.J. Lippard, *J. Am. Chem. Soc.* 98 (1976) 5720;
(b) C.-L.O. Young, J.C. Dewan, H.R. Lienthal, S.J. Lippard, *J. Am. Chem. Soc.* 100 (1978) 7291;
(c) P.K. Coughlin, J.C. Dewan, S.J. Lippard, E. Watanabe, J.-M. Lehn, *J. Am. Chem. Soc.* 101 (1979) 265;
(d) G. Kolks, C.R. Frihart, P.K. Coughlin, S.J. Lippard, *Inorg. Chem.* 20 (1981) 2933;
(e) P.K. Coughlin, A.E. Martin, J.C. Dewan, E. Watanabe, J.E. Bulkowski, J.-M. Lehn, S.J. Lippard, *Inorg. Chem.* 23 (1984) 1004;
(f) P.K. Coughlin, S.J. Lippard, *Inorg. Chem.* 23 (1984) 1446.
- (a) M. Sato, S. Nagae, M. Uehara, J. Nakaya, *J. Chem. Soc. Chem. Commun.* (1984) 1661;
(b) Q. Lu, Q.H. Luo, A.B. Dai, Z.Y. Zhou, G.Z. Hu, *J. Chem. Soc. Chem. Commun.* (1990) 1429;
(c) M. Zongwan, C. Dong, T. Wenxia, Y. Kaibei, L. Li, *Polyhedron* 11 (1992) 191;
(d) J.-L. Pierre, P. Chautemps, S. Refaif, C. Beguin, A.E. Marzouki, G. Serratrice, E. Saint-Aman, P. Rey, *J. Am. Chem. Soc.* 117 (1995) 1965;
(e) Z.-W. Mao, M.-Q. Chen, X.-S. Tan, J. Liu, W.-X. Tang, *Inorg. Chem.* 34 (1995) 2889.
- J.A. Tainer, E.D. Getzoff, J.S. Richardson, D.C. Richardson, *Nature* 306 (1983) 284.
- M. Harata, K. Jitsukawa, H. Masuda, H. Einaga, *J. Am. Chem. Soc.* 116 (1994) 10817.
- M. Harata, K. Jitsukawa, H. Masuda, H. Einaga, *Chem. Lett.* (1995) 61.
- M. Harata, K. Jitsukawa, H. Masuda, H. Einaga, *Chem. Lett.* (1996) 813.
- (a) A.S. Potapov, E.A. Nudnova, G.A. Domina, L.N. Kirpotina, M.T. Quinn, A.I. Khlebnikov, I.A. Schepetkin, *Dalton Trans.* (2009) 4488;
(b) C. Metcalfe, J.A. Thomas, *Chem. Soc. Rev.* 32 (2003) 215;
(c) H. Chao, L.N. Ji, *Bioinorg. Chem. Appl.* 3 (2005) 15.
- (a) E. Bienvenue, S. Choua, M.A. Lobo-Recio, C. Marzin, P. Pacheco, P. Seta, et al., *J. Inorg. Biochem.* 57 (1995) 157;
(b) E.K. Efthimiadou, Y. Sanakis, M. Katsarou, C.P. Raptopoulou, A. Karaliota, N. Katsaros, G. Psomas, *J. Inorg. Biochem.* 100 (2006) 21;
(c) D. Lahiri, T. Bhowmick, B. Banik, R. Railkar, S. Ramakumar, R.R. Dighe, A.R. Chakravarty, *Polyhedron* 29 (2010) 2417.
- (a) A.R. Chakravarty, P.A. Reddy, B.K. Santra, A.M. Thomas, *Proc. Indian Acad. Sci. (Chem. Sci.)* 114 (2002) 391;
(b) M.D. Kuwabara, C. Yoon, T.E. Goyne, T. Thederahn, D.S. Sigman, *Biochemistry* 25 (1986) 7401.
- M.J.S. Moreno, A.F. Botello, R.B.G. Coca, R. Griesser, J. Ochocki, A. Kotynski, J.N. Gutierrez, V. Moreno, H. Sigel, *Inorg. Chem.* 43 (2004) 1311.
- A. Hori, K. Kubo, M. Kusaka, *Cancer Lett.* 183 (2002) 53.
- M. Harata, K. Hasegawa, K. Jitsukawa, H. Masuda, H. Einaga, *Bull. Chem. Soc. Jpn.* 71 (1998) 1031.
- S. Thyagarajan, N.N. Murthy, A.A.N. Sarjean, K.D. Karlin, S.E. Rokita, *J. Am. Chem. Soc.* 128 (2006) 7003.
- J.R. Morrow, O. Iranzo, *Curr. Opin. Chem. Biol.* 8 (2004) 192.
- (a) P. Carloni, E. Peter, P.E. Blochl, E. Parrinello, *J. Phys. Chem.* 99 (1995) 1338;
(b) R. Osman, H. Basch, *J. Am. Chem. Soc.* 106 (1984) 5710;
(c) M. Rosi, A. Sgamellotti, F. Tarantelli, I. Bertini, C. Luchinat, *Inorg. Chim. Acta* 107 (1985) L21.
- L. Naso, A.C.G. Baro, L. Lezama, T. Rojo, P.A.M. Williams, *J. Inorg. Biochem.* 103 (2009) 219.
- A. Klanicova, Z. Travnicka, J. Vanco, I. Popa, Z. Sindelar, *Polyhedron* 29 (2010) 2582.
- K. Singh, P. Patel, B.V. Agarwala, *Spectrosc. Lett.* 28 (1995) 747.
- O. Pouralimardan, A.-C. Chamayou, C. Janiak, H. H.-Monfared, *Inorg. Chim. Acta* 360 (2007) 1599.
- R.C. Maurya, J. Chourasia, P. Sharma, *Indian J. Chem. A* 47 (2008) 517.
- (a) D. Martini, M. Pellei, C. Pettinari, B.W. Skelton, A.H. White, *Inorg. Chim. Acta* 333 (2002) 72;
(b) D. Czakis-Sulikowska, A. Czynkowska, *J. Therm. Anal. Cal.* 76 (2004) 54;
(c) G.B. Deacon, R.J. Phillips, *Coord. Chem. Rev.* 33 (1980) 227.
- S. Chandra, D. Jain, A.K. Sharma, P. Sharma, *Molecules* 14 (2009) 174.
- M. Nara, M. Tasumi, M. Tanokura, T. Hiraoki, M. Yazawa, A. Tsutsumi, *FEBS Lett.* 349 (1994) 84.
- P.R. Reddy, A.M. Reddy, *Indian J. Chem.* 41A (2002) 2083.
- A.C. Testa, *Spectrochim. Acta Part. A* 55 (1999) 2393.
- Q. Chu, Y. Wang, S. Zhu, *Synth. Commun.* 30 (2000) 677.
- A. Taha, *Spectrochim. Acta Part. A* 59 (2003) 1611.
- (a) M. Devereux, D.O. Shea, A. Kellett, M. McCann, M. Walsh, D. Egan, C. Deegan, K. Kedziora, G. Rosair, H. M.-Bunz, *J. Inorg. Biochem.* 101 (2007) 881;
(b) R. Huang, A. Wallqvist, D.G. Covell, *Biochem. Pharmacol.* 100 (2006) 1389;
(c) S. Dhar, M. Nethaji, A.R. Chakravarty, *Inorg. Chem.* 44 (2005) 8876.
- (a) E.K. Efthimiadou, N. Katsaros, A. Karaliota, G. Psomas, *Inorg. Chim. Acta* 360 (2007) 4093;
(b) F.E. Mabbs, D. Collison, *Electron Paramagnetic Resonance of d Transition Metal Compounds*, Elsevier, Amsterdam, 1992.
- M. Vaidyanathan, R. Viswanathan, M. Palaniandavar, T. Balasubramanian, P. Prabhakaran, T.P. Muthiah, *Inorg. Chem.* 37 (1998) 6418.
- (a) E. Garribba, G. Micera, *J. Chem. Educ.* 83 (2006) 1229;
(b) P.U. Maheswari, M. van der Ster, S. Smulders, S. Barends, G.P. van Wezel, C. Massera, S. Roy, H. den Dulk, P. Gamez, J. Reedijk, *Inorg. Chem.* 47 (2008) 3719.
- R. Balamurugan, M. Palaniandavar, R.S. Gopalan, G.U. Kulkarni, *Inorg. Chim. Acta* 357 (2004) 919.
- M. Chauhan, K. Banerjee, F. Arjmand, *Inorg. Chem.* 46 (2007) 3072.
- (a) A.M. Pyle, E.C. Long, J.K. Barton, *J. Am. Chem. Soc.* 111 (1989) 4520;
(b) A. Sitlani, E.C. Long, A.M. Pyle, J.K. Barton, *J. Am. Chem. Soc.* 114 (1992) 2303.

- [45] J.K. Barton, J.M. Goldberg, C.V. Kumar, N.J. Turro, *J. Am. Chem. Soc.* 108 (1986) 2081.
- [46] E.K. Efthimiadou, A. Karaliota, G. Psomas, *J. Inorg. Biochem.* 104 (2010) 455.
- [47] P.J. Cox, G. Psomas, C.A. Bolos, *Bioorg. Med. Chem.* 17 (2009) 6054.
- [48] E.C. Long, J.K. Barton, *Acc. Chem. Res.* 23 (1990) 271.
- [49] C.V. Kumar, J.K. Barton, N.J. Turro, *J. Am. Chem. Soc.* 107 (1985) 5518.
- [50] F. Dimiza, F. Perdih, V. Tangoulis, I. Turel, D.P. Kessissoglou, G. Psomas, *J. Inorg. Biochem.* 105 (2011) 476.
- [51] F. Arjmand, S. Parveen, M. Afzal, L. Toupet, T.B. Hadda, *Eur. J. Med. Chem.* 49 (2012) 141.
- [52] J. Liu, T. Zhang, T. Lu, L. Qu, H. Zhou, Q. Zhang, L. Ji, *J. Inorg. Biochem.* 91 (2002) 269.
- [53] J. Liu, H. Zhang, C. Chen, H. Deng, T. Lu, L.N. Ji, *J. Chem. Soc. Dalton Trans.* (2003) 114.
- [54] F. Arjmand, F. Sayeed, M. Muddassir, *J. Photochem. Photobiol. B* 103 (2011) 166.
- [55] F. Boussicault, M. Robert, *Chem. Rev.* 108 (2008) 2622.
- [56] Z.S. Yang, Y.L. Wang, Y.C. Liu, G.C. Zhao, *Anal. Sci.* 21 (2005) 1355.
- [57] (a) M.T. Carter, M. Rodriguez, A.J. Bard, *J. Am. Chem. Soc.* 111 (1989) 8901; (b) G. Psomas, *J. Inorg. Biochem.* 102 (2008) 1798; (c) K. Jiao, Q.X. Wang, W. Sun, F.F. Jian, *J. Inorg. Biochem.* 99 (2005) 1369; (d) S. Tabassum, I.-u-H. Bhat, F. Arjmand, *Spectrochim. Acta A* 74 (2009) 1152.
- [58] M. Jain, R.V. Singh, *Bioinorg. Chem. Appl.* 2006 (2006) 1.
- [59] G. Lupidi, F. Marchetti, N. Masciocchi, D.L. Reger, S. Tabassum, P. Astolfi, E. Damiani, C. Pettinari, *J. Inorg. Biochem.* 104 (2010) 820.
- [60] J.-W. Park, S.M. Lee, *J. Biochem. Mol. Biol.* 28 (1995) 249.
- [61] T. Ohse, S. Nagaoka, Y. Arakawa, H. Kawakami, K. Nakamura, *J. Inorg. Biochem.* 85 (2001) 201.
- [62] C.A. Detmer III, F.V. Pamatong, J.R. Bocarsly, *Inorg. Chem.* 36 (1997) 3676.
- [63] C.A. Detmer III, F.V. Pamatong, J.R. Bocarsly, *Inorg. Chem.* 35 (1996) 6292.
- [64] A. Mazumder, C.L. Sutton, D.S. Sigman, *Inorg. Chem.* 32 (1993) 3516.
- [65] M. González-Alvarez, G.A.J. Borras, M. Pitie, B. Meunier, *J. Biol. Inorg. Chem.* 8 (2003) 644.
- [66] E. Trotta, N.D. Grosso, M. Erba, M. Paci, *Biochemistry* 39 (2000) 6799.
- [67] P. Wittung, P. Nielsen, B. Norden, *J. Am. Chem. Soc.* 118 (1996) 7049.
- [68] D. Kovala-Demertzi, M. Staninska, I. Garcia-Santos, A. Castineiras, M.A. Demertzis, *J. Inorg. Biochem.* 105 (2011) 1187.
- [69] G. Asgedom, A. Sreedhara, J. Kivikoski, J. Valkonen, C.P. Rao, *Dalton Trans.* (1995) 2459.
- [70] (a) M. Eriksson, M. Leijon, C. Hiort, B. Norden, A. Graslund, *Biochemistry* 33 (1994) 5031; (b) F. Arjmand, M. Chauhan, *Helv. Chim. Acta* 88 (2005) 2413.
- [71] J. Marmur, *J. Mol. Biol.* 3 (1961) 208.
- [72] M.E. Reicmann, S.A. Rice, C.A. Thomas, P. Doty, *J. Am. Chem. Soc.* 76 (1954) 3047.
- [73] R. L.Dutta, A. Syamal, *Elements of Magneto Chemistry*, second ed., Affiliated East-West Press, New Delhi, 1993, 8.
- [74] Y. Iwamoto, J. Mifuchi, *Chem. Pharm. Bull.* 30 (1982) 237.
- [75] G. Singh, S. Maurya, M.P. Lampasona, C.A.N. Catalan, *Food Chem. Toxicol.* 45 (2007) 1650.
- [76] J.M. Vincent, *Nature* 189 (1947) 1373.
- [77] A. Gangjee, O.A. Namjoshi, S.N. Keller, C.D. Smith, *Bioorg. Med. Chem.* 19 (2011) 4355.